# Particle acceleration at forward and reverse shocks in SNRs

V.N.Zirakashvili

Pushkov Institute of Terrestrial Magnetism, Ionosphere and Radiowave Propagation, Russian Academy of Sciences (IZMIRAN), 108840 Troitsk, Moscow, Russia

# Outline

- Diffusive shock acceleration (DSA) of particles in SNRs
- Amplification of magnetic fields and electric effects in young SNRs
- Modeling of DSA in young and old SNRs
- IIn supernova as the sources of high energy astrophysical neutrinos

# Diffusive Shock Acceleration

Krymsky 1977; Bell 1978; Axford et al.1977; Blandford & Ostriker 1978

Very attractive feature: power-law spectrum of particles accelerated, $\gamma=(\sigma+2)/(\sigma-1)$, where $\sigma$ is the shock compression ratio, for strong shocks $\sigma=4$ and $\gamma=2$

Maximum energy for SN: $D\sim 0.1 u_{sh} R_{sh}$

$\sim 3\cdot 10^{27}$ cm$^2$/s $< D_{gal}$

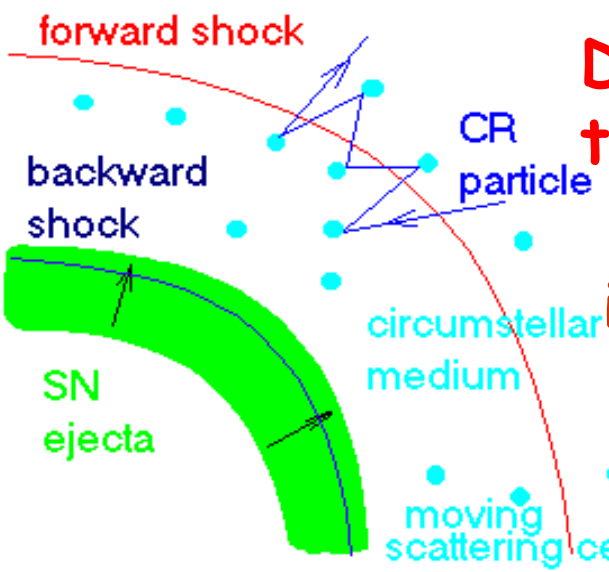


Diffusion coefficient should be small in the vicinity of SN shock

In the Bohm limit $D=D_B=cr_g/3$ and for interstellar magnetic field

$$E_{\max} = Z\cdot 10^{14}\,\mathrm{eV}\left(\frac{B}{10\,\mu\mathrm{G}}\right)\left(\frac{R_{\mathrm{sh}}}{3\,\mathrm{pc}}\right)\left(\frac{u_{\mathrm{sh}}}{3000\,\mathrm{km\,s^{-1}}}\right)$$

# X-ray image of Tycho SNR (from Warren et al. 2005)

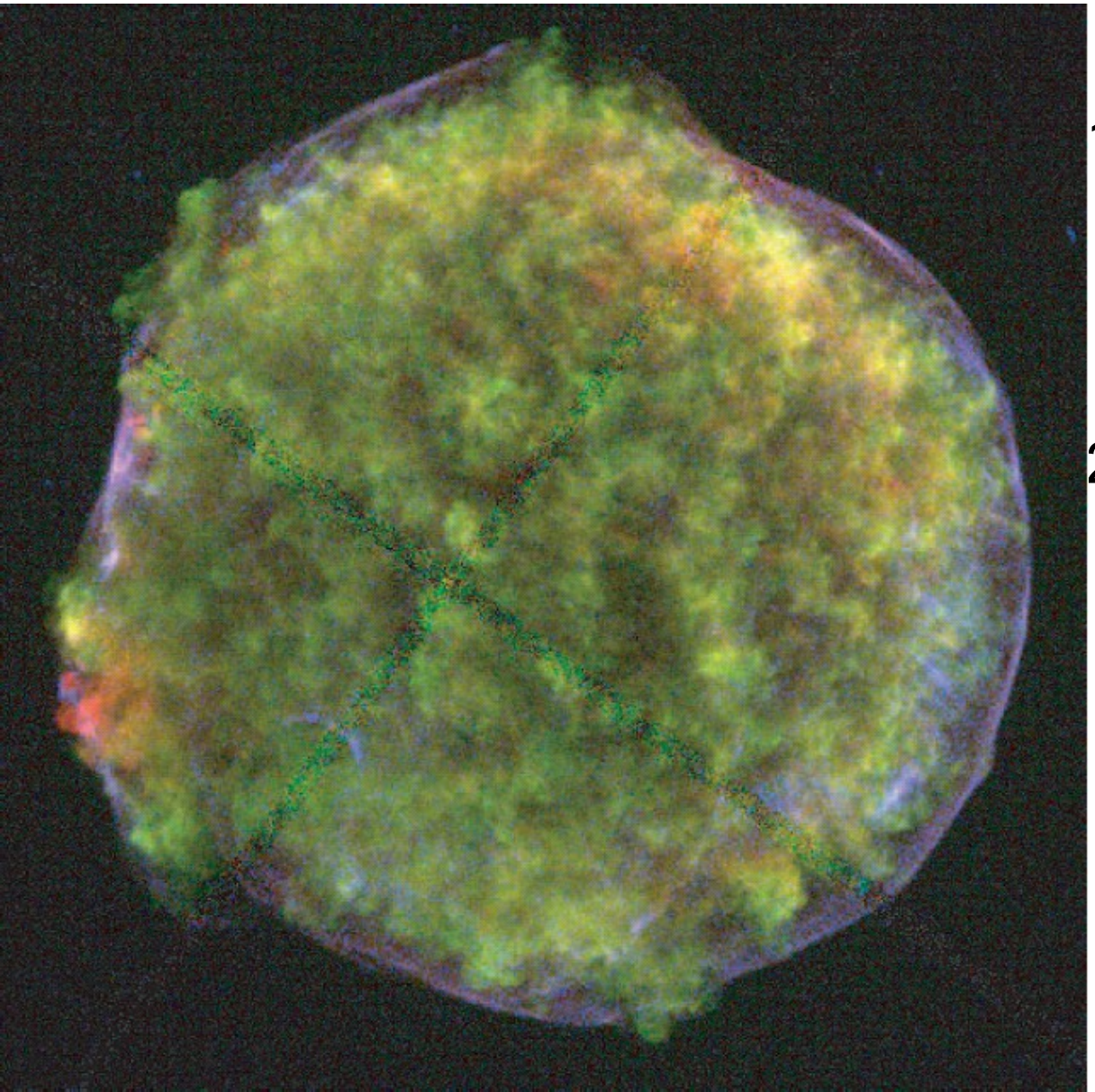

1. CD is close to the forward shock – evidence of the shock modification by CR pressure.
2. Thin non-thermal X-ray filaments at the periphery of the remnant – evidence of electron acceleration and of magnetic amplification.

# Magnetic field amplification by non-resonant streaming instability

Bell (2004) used Achterberg's results (1983) and found the regime of instability that was overlooked

$$F_{CR} = -\frac{1}{c}\left[j_d \times B\right]$$

$$\omega^2 = V_a^2 k^2 - j_d \frac{B_0 k}{c\rho_0}$$

$$k\, r_g >> 1,\ \gamma_{max} = j_d B_0 / 2c\rho V_a$$

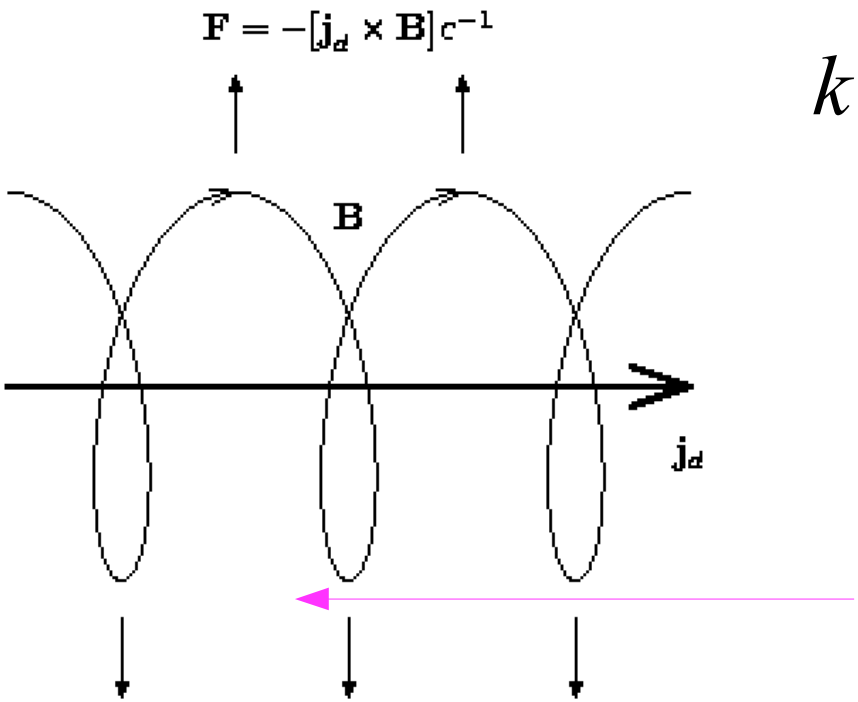


Since the CR trajectories are weakly influenced by the small-scale field, the use of the mean $j_d$ is well justified

**E**= - [**u**X**B**]/c

Regular electric field

# Modeling of Bell's instability (Matthews et al. 2017)

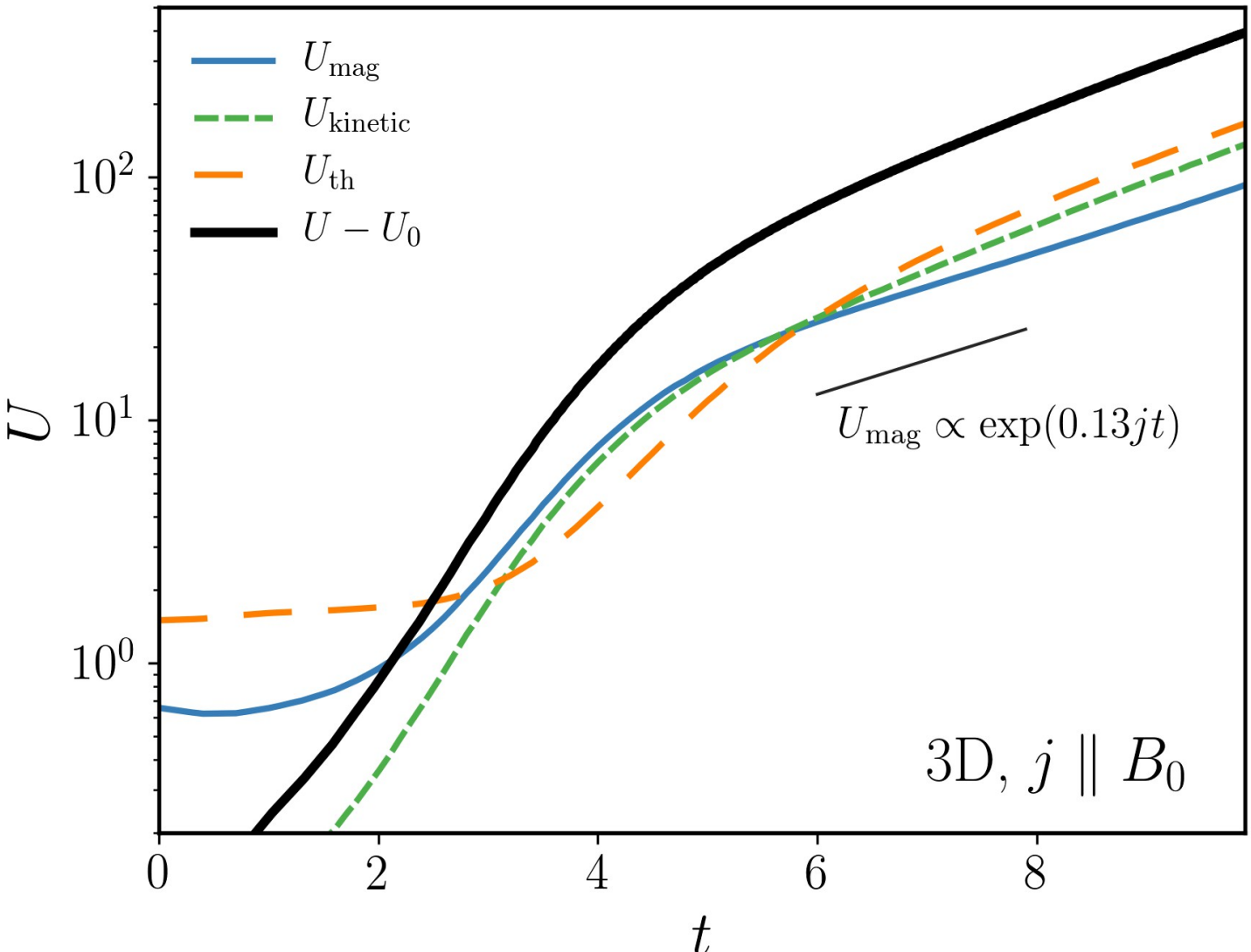


Exponential nonlinear growth (Beresnyak & Li 2014) was confirmed.

This is important for small initial $B_0$ e.g. at reverse shocks in SNRs

# MHD modeling in the shock transition region and downstream of the shock

Zirakashvili & Ptuskin 2008

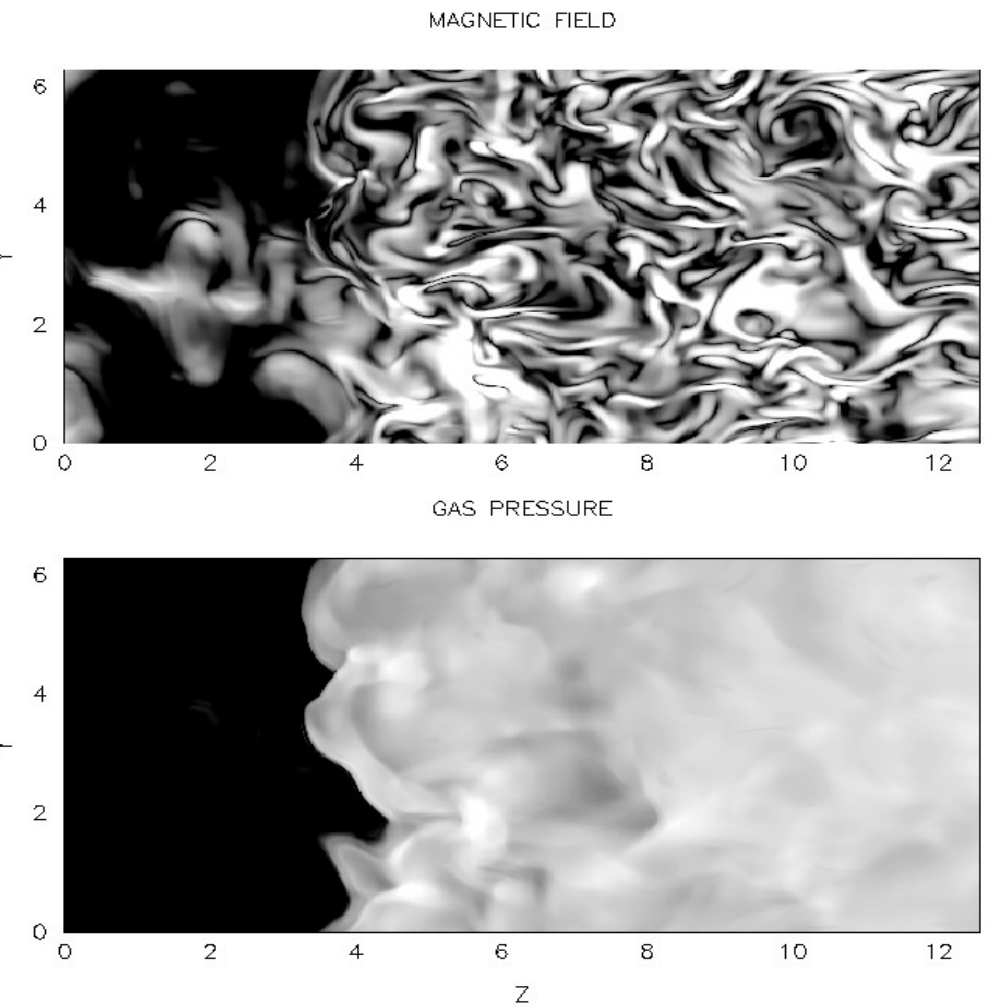


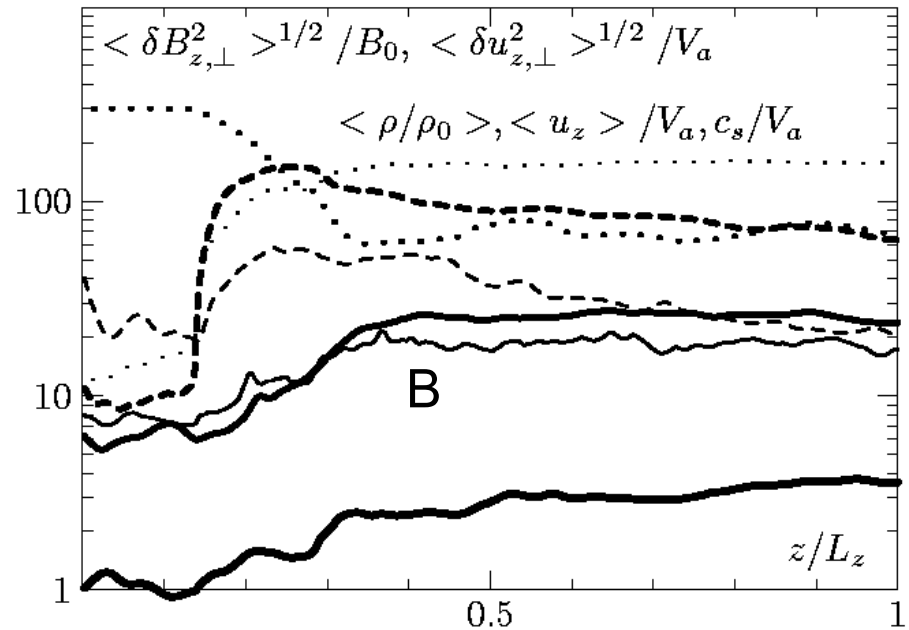


$u_1$=3000 km/s $V_a$=10 km/s

$\eta_{esc}$=0.14

0.02L

Magnetic field is not damped and is perpendicular to the shock front downstream of the shock!

Ratio=1.4 $\sigma_B$=3

3D $256^2 \times 512$

Wood & Mufson 1992

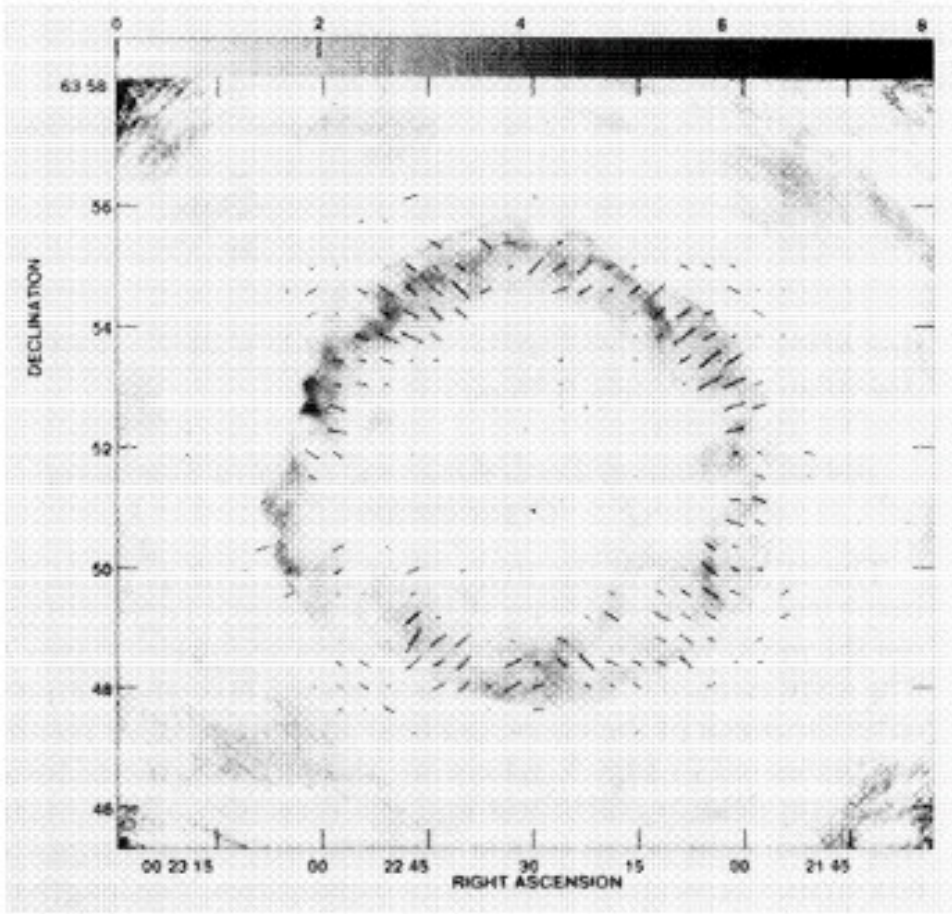


Dickel et al. 1991

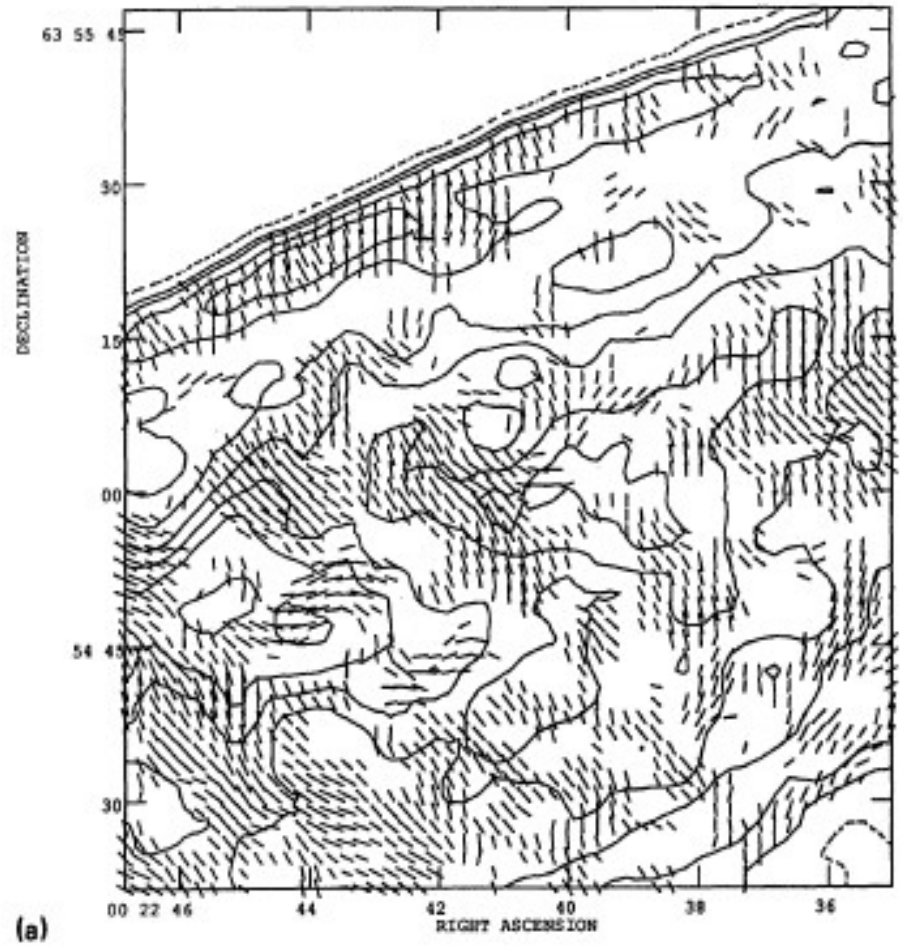


FIG. 5. Map of the remnant of Tycho's supernova showing local magnetic field organization and the direction of the mean local field averaged over boxes of various sizes, superposed on total intensity grey scale as shown in Dickel *et al.* 1991 (Paper I). The length of the vectors indicates the degree of organization in a box, and is proportional to $\Upsilon_{org}$. The angle of the vector corresponds to the alignment of the mean magnetic field in a box. Positive values of the total intensity are represented with a peak of $8.1\times10^{-3}$ Jy beam$^{-1}$; the grey scale is in units of $10^{-3}$ Jy beam$^{-1}$. (a) Box size of $30\times30$ pixels (0.55 pc$\times$0.55 pc). (b) Box size of $15\times15$ pixels (0.27 pc$\times$0.27 pc).

Radial magnetic fields were indeed observed in young SNRs

# Simple estimate of electric effects

$$W = q\mathbf{E}\mathbf{J}_d = -4\pi \int p^2 dpq\mathbf{E}D\nabla N =$$

Energy losses

$$-\frac{4\pi}{3}\mathbf{V_{A0}} \int p^2 dpvp(r_{g0}k)\nabla N$$

$$\mathbf{E} = \frac{\mathbf{V_{A0}}}{c}\frac{\delta B^2}{B_0}$$

$$D = D_{B0} k r_{g0} \frac{B_0^2}{\delta B^2}$$

Small-scale scattering

$$V_{eff} = V_{A0} r_{g0} k = r_{g0}\gamma \sim \frac{10}{T} r_{g0} \sim 10u\frac{r_{g0}}{R}$$

Effective CR velocity is higher than Alfven velocity in the amplified field

$$r_{g0} < 0.1R$$

Limitation of maximum energy

# Modeling of DSA with electric field at the plane shock (Zirakashvili & Ptuskin 2015)

$$\frac{\partial N}{\partial t} = \left( \frac{\partial}{\partial z} + \frac{1}{p^2} \frac{\partial}{\partial p} p^2 \frac{qE_{el}}{\mathrm{v}} \right) D \left( \frac{\partial N}{\partial z} + \frac{qE_{el}}{\mathrm{v}} \frac{\partial N}{\partial p} \right) - u \frac{\partial N}{\partial z} + \frac{p}{3} \frac{\partial N}{\partial p} \frac{\partial u}{\partial z}$$

$$D = \frac{\mathrm{v} p^2 c^2}{12\pi q^2} \Big/ \int W(k) dk / k$$

$$\frac{\partial W}{\partial t} + u \frac{\partial W}{\partial z} = 2(\Gamma_B - \Gamma_{NL}) W$$

$$\Gamma_B = \sqrt{\frac{j_d B_0 k}{c\rho} - V_A^2 k^2} \qquad \Gamma_{NL} = 0.2\, V_A k \left( \frac{k W(k)}{B_0^2 / 4\pi} \right)^{1/2}$$

$$j_d = q \int 4\pi p^2 dp J_d(p) \qquad E_{el} = \frac{4\pi}{c B_0} \int dk \left( \Gamma_B - \Gamma_{NL} \right) W(k) / k$$

# Numerical results

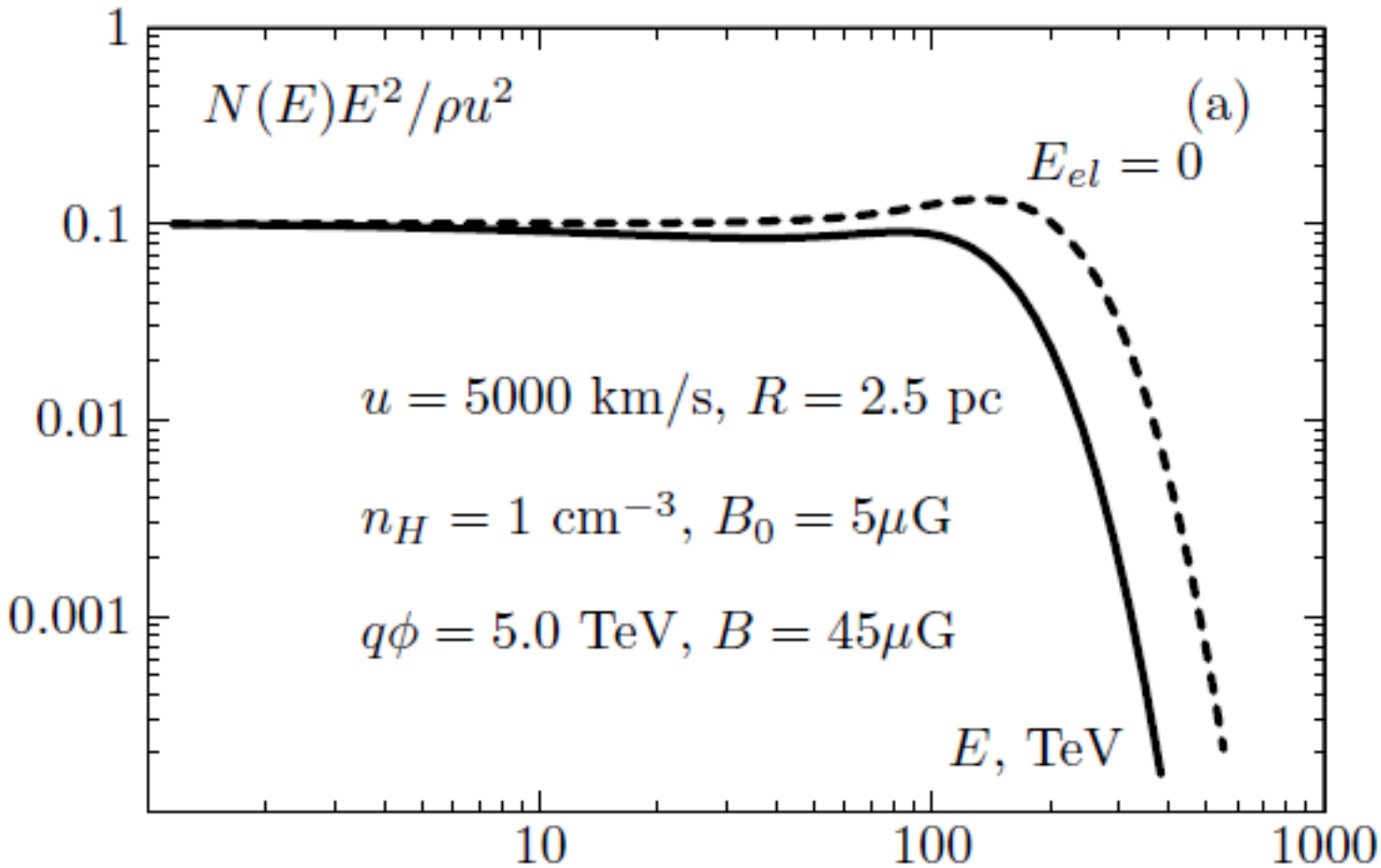

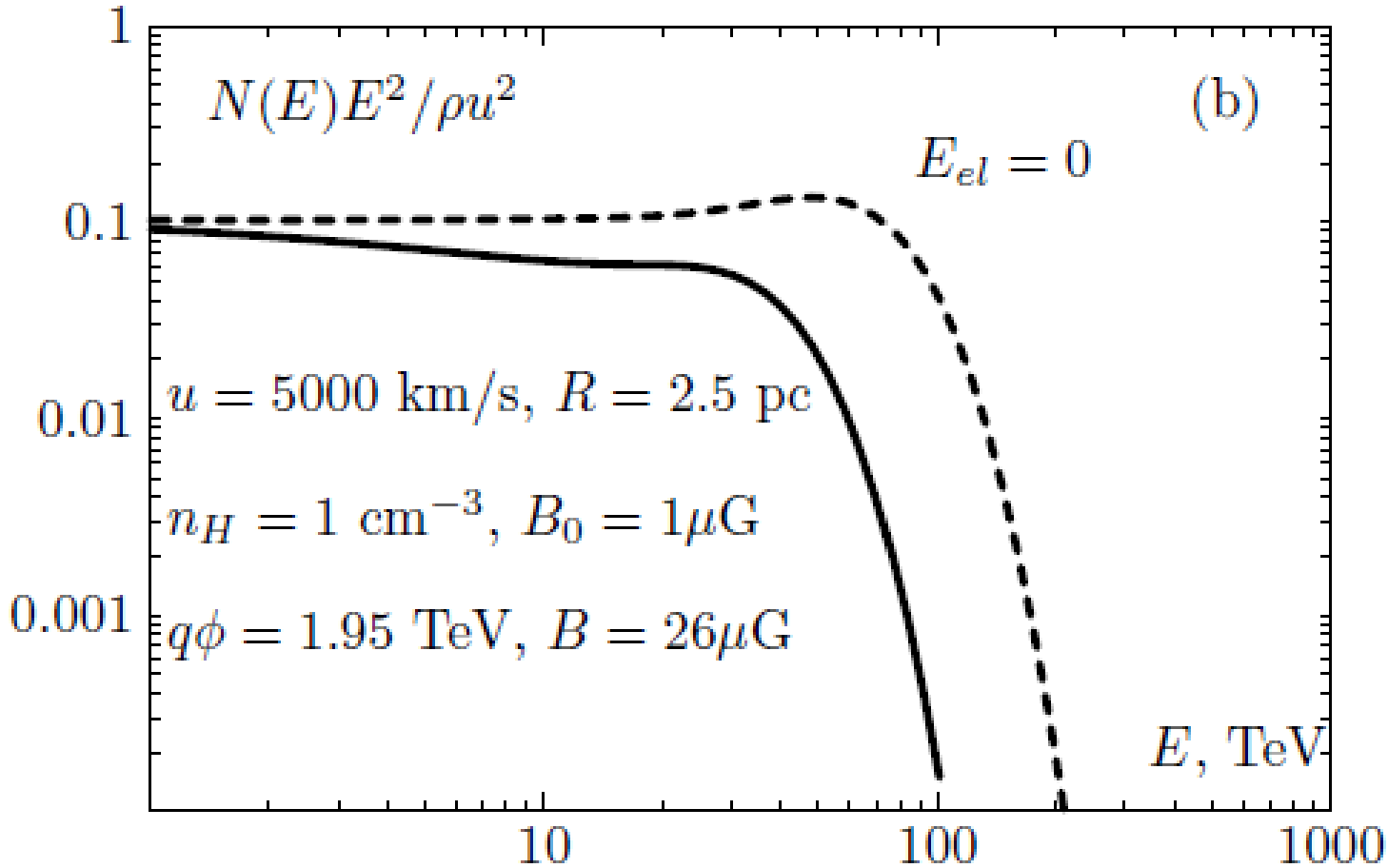
$N(E)E^2/\rho u^2$
(b)
$E_{el} = 0$
$u = 5000$ km/s, $R = 2.5$ pc
$n_H = 1$ cm$^{-3}$, $B_0 = 1\mu$G
$q\phi = 1.95$ TeV, $B = 26\mu$G
$E$, TeV
1
0.1
0.01
0.001
10
100
1000

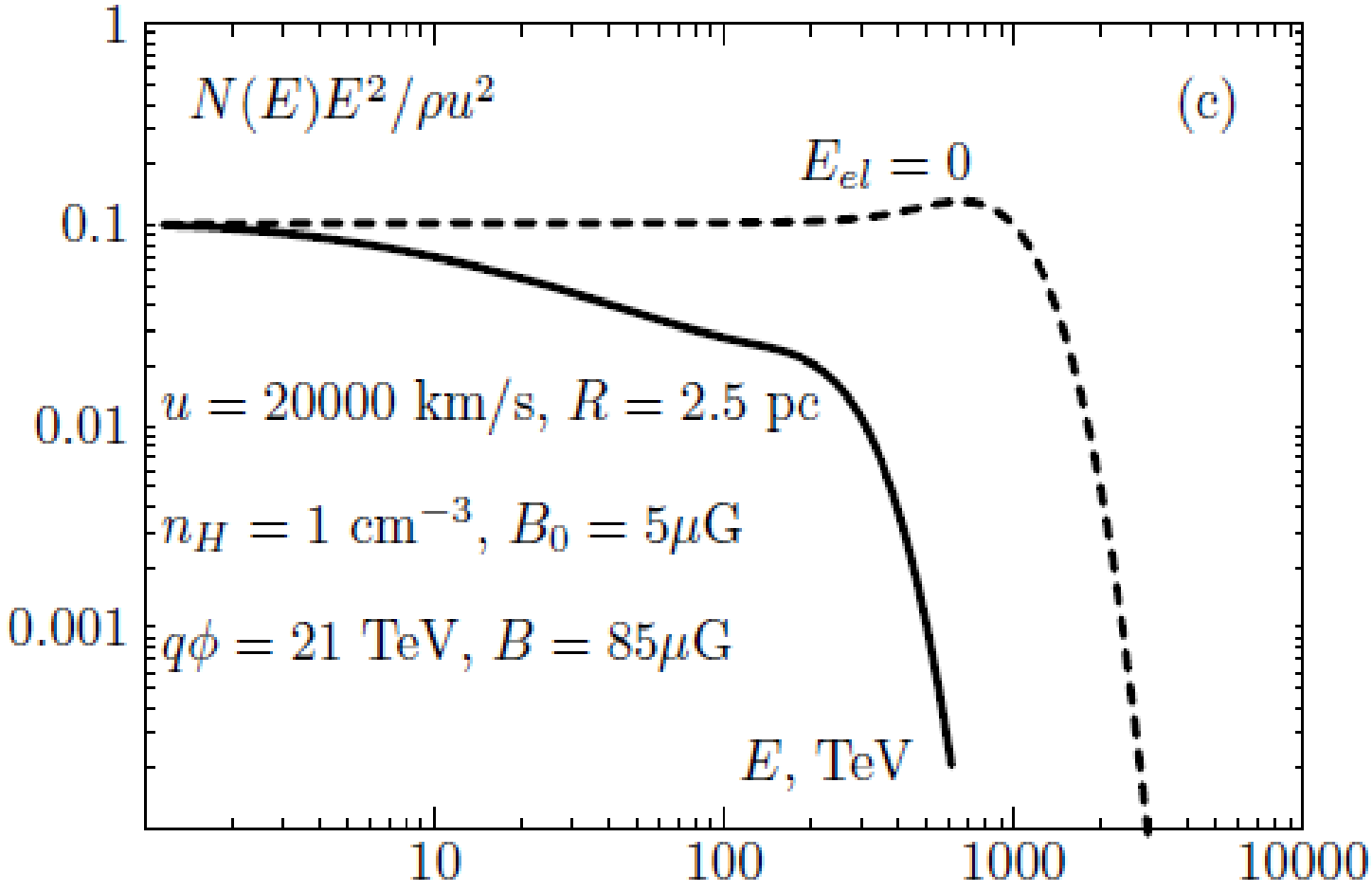
$N(E)E^2/\rho u^2$
(c)
$E_{el} = 0$
$u = 20000$ km/s, $R = 2.5$ pc
$n_H = 1$ cm$^{-3}$, $B_0 = 5\mu$G
$q\phi = 21$ TeV, $B = 85\mu$G
$E$, TeV
1
0.1
0.01
0.001
10
100
1000
10000

# TeV gamma-rays from young SNRs

Aharonian et al 2008 (HESS)

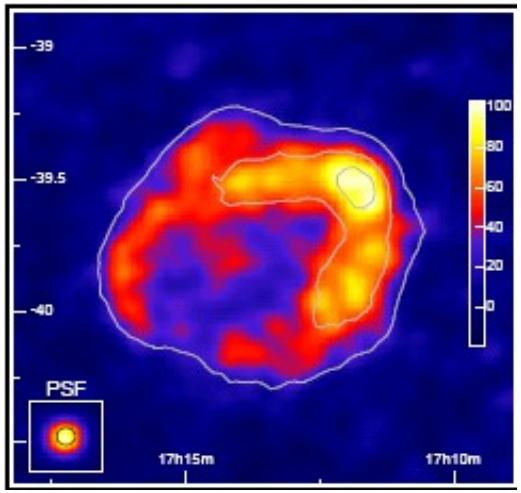


Particles accelerated up to100 TeV in these SNRs. Gamma-rays can be produced in pp collisions (hadronic models) or via the Inverse Compton scattering of IR and MWBR photons on the electrons accelerated (leptonic models)

Aharonian et al 2007 (HESS)

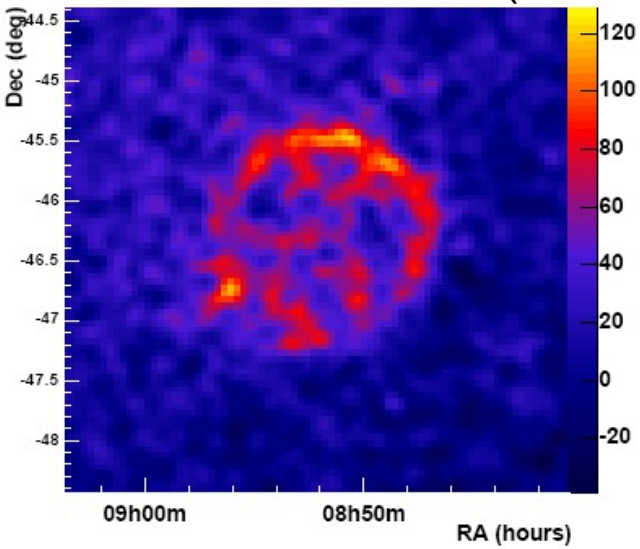


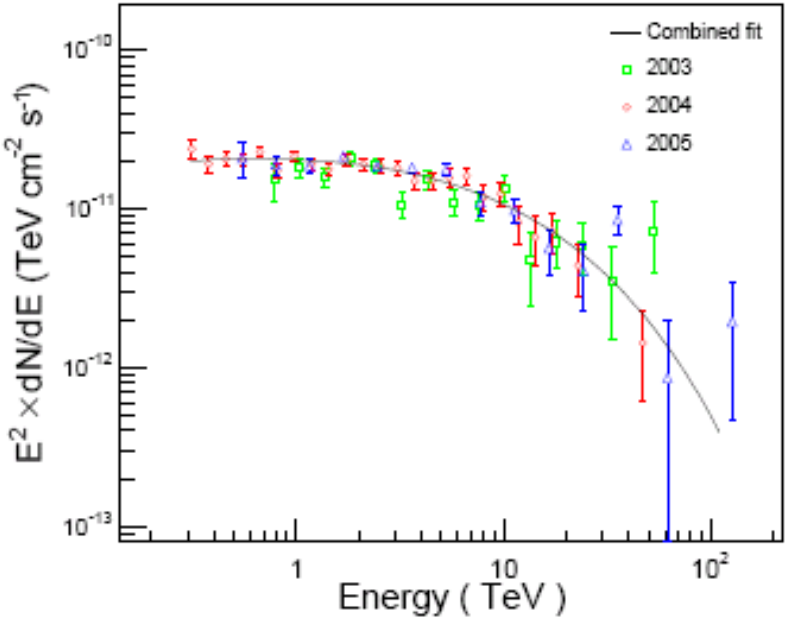


RX J1713.7-3946

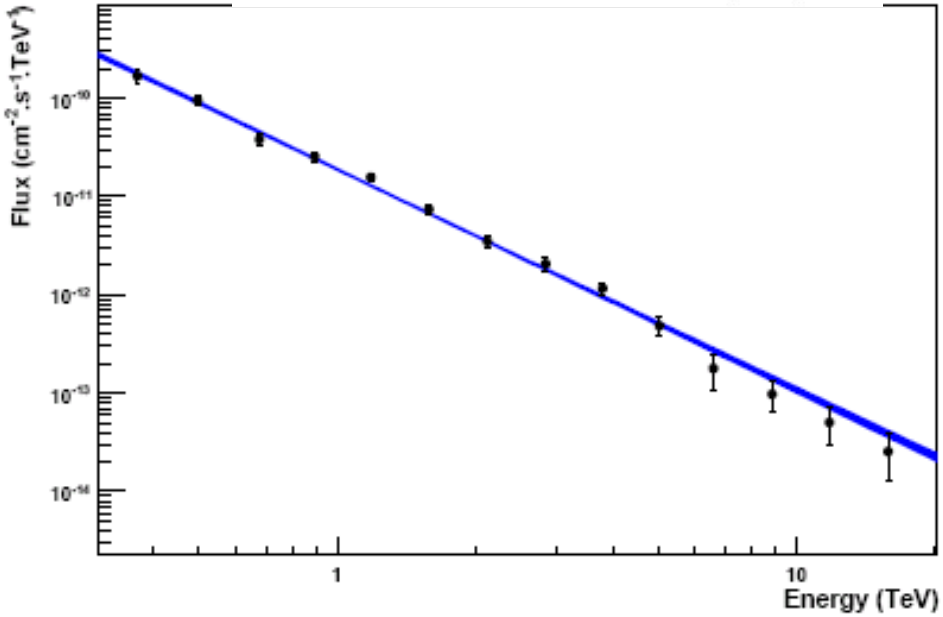


Vela Jr

# Numerical model of nonlinear diffusive shock acceleration

(Zirakashvili & Ptuskin 2012)

(natural development of existing models of Berezhko et al. (1994-2006), Kang & Jones 2006, see also half-analytical models of Blasi et al.(2005); Ellison et al. (2010) )

$$\frac{\partial \rho}{\partial t} = -\frac{1}{r^2}\frac{\partial}{\partial r} r^2 u \rho \qquad (1)$$

$$\frac{\partial u}{\partial t} = -u\frac{\partial u}{\partial r} - \frac{1}{\rho}\left(\frac{\partial P_g}{\partial r} + \frac{\partial P_c}{\partial r}\right) \qquad (2)$$

$$\frac{\partial P_g}{\partial t} = -u\frac{\partial P_g}{\partial r} - \frac{\gamma_g P_g}{r^2}\frac{\partial r^2 u}{\partial r} - (\gamma_g - 1)(w-u)\frac{\partial P_c}{\partial r} \qquad (3)$$

$$\frac{\partial N}{\partial t} = \frac{1}{r^2}\frac{\partial}{\partial r} r^2 D(p,r,t)\frac{\partial N}{\partial r} - w\frac{\partial N}{\partial r} + \frac{\partial N}{\partial p}\frac{p}{3r^2}\frac{\partial r^2 w}{\partial r}$$

$$+\frac{\eta_f \delta(p-p_f)}{4\pi p_f^2 m}\rho(R_f+0,t)(\dot{R}_f - u(R+0,t))\delta(r-R_f(t))$$

$$+\frac{\eta_b \delta(p-p_b)}{4\pi p_b^2 m}\rho(R_b-0,t)(u(R_b-0,t) - \dot{R}_b)\delta(r-R_b(t))$$

$$(4)$$

Spherically symmetric HD equations + CR transport equation

Acceleration at forward and reverse shocks

# CR acceleration at the reverse shock (e.g.Ellison et al. 2005) ?

# Probably presents in Cas A

(Helder & Vink 2008)

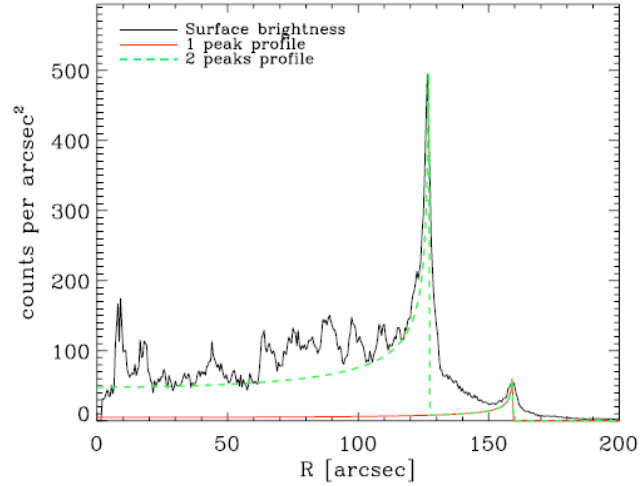


FIG. 3.— Radial surface brightness profile (smooth solid line) in the 4.2 to 6.0 keV energy band at an angle of 10° to 30° (including the featureless filament found by Hughes et al. (2000)). The smooth solid line indicates what the profile will look like if the surface brightness is produced by an emissivity function with only a peak at the outer shock. For the dashed line, we use an emissivity function with two peaks. Note that this is not a fit, just an illustrative example.

Magnetic field of ejecta?

$B \sim R^{-2}$, $10^4$G at $R=10^{13}$ cm -

$10^{-8}$G at $R=10^{19}$cm=3pc

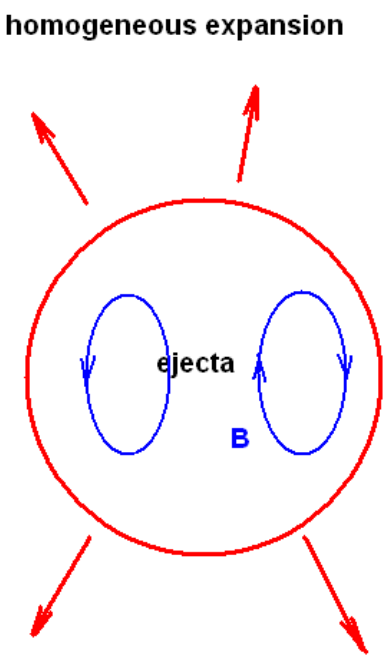


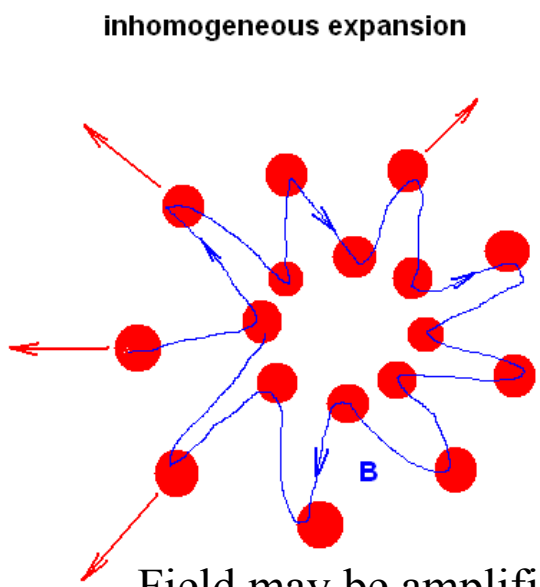


+additional amplification by the non-resonant streaming instability (Bell 2004)

Field may be amplified and become radial – enhanced ion injection at the reverse shock

Radio-image of Cas A

Atoyan et al. 2000

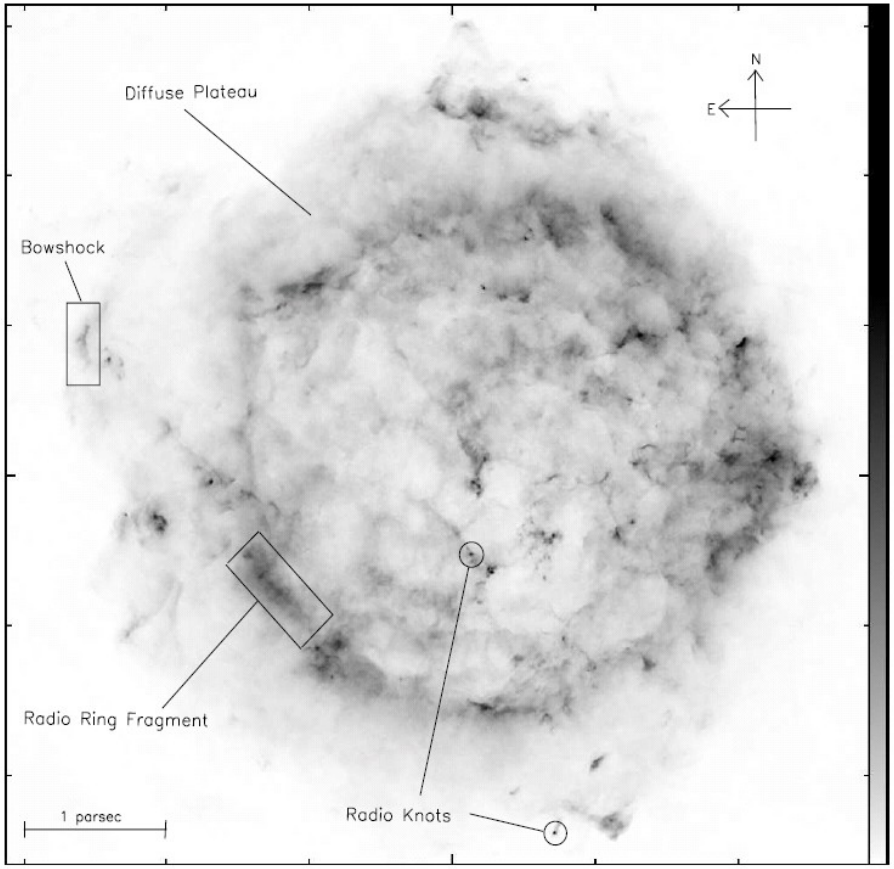


X-ray image of Cas A (Chandra)

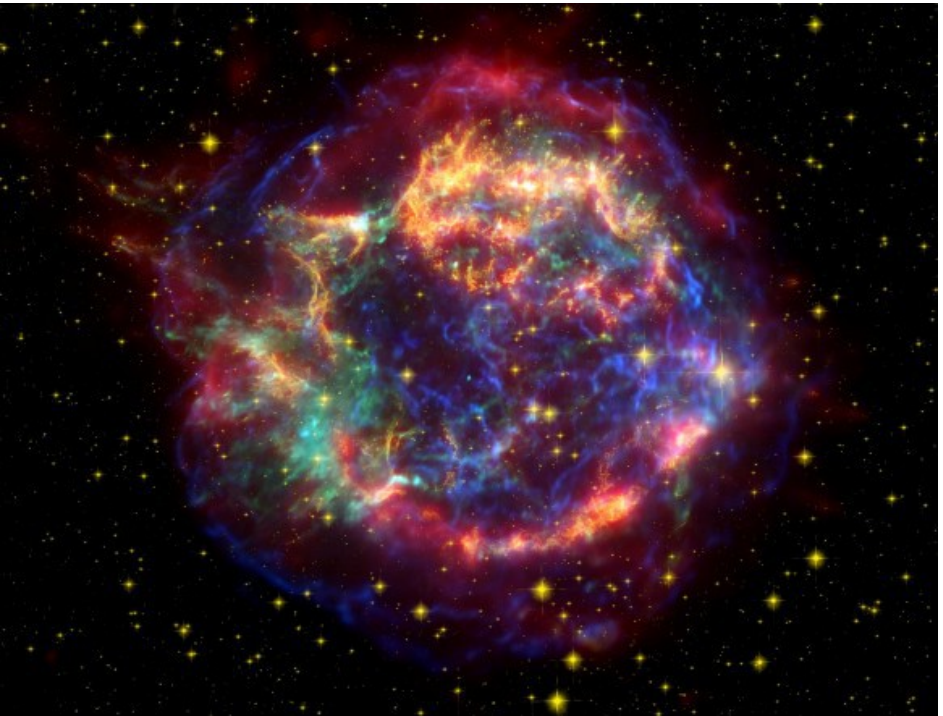

Inner bright radio- and X-ray-ring is related with the reverse shock of Cas A while the diffuse radio-plateau and thin outer X-ray filaments are produced by electrons accelerated at the forward shock.

# Radio-image of RX J1713.7-3946 (Lazendic et al. 2004)

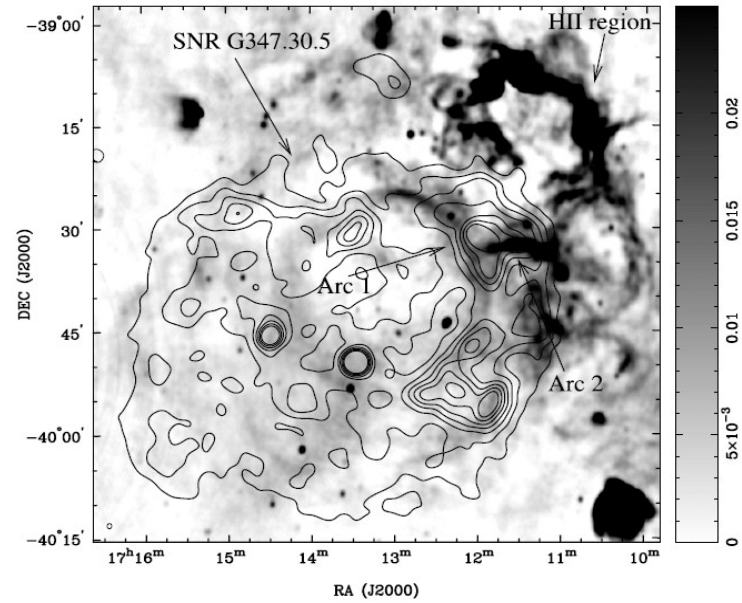


FIG. 5.—ATCA images of G347.3−0.5 and surrounding region at 1.4 GHz. The image was convolved with a Gaussian restoring beam of 46″ × 36″ (P.A. = −3°8), shown by the tiny ellipse in the bottom left-hand corner. The image is overlaid with the *ROSAT* contours with the same levels as in Fig. 1. The linear gray scale is in units of Jy beam$^{-1}$.

# X-rays: XMM-Newton, Acero et al. 2009

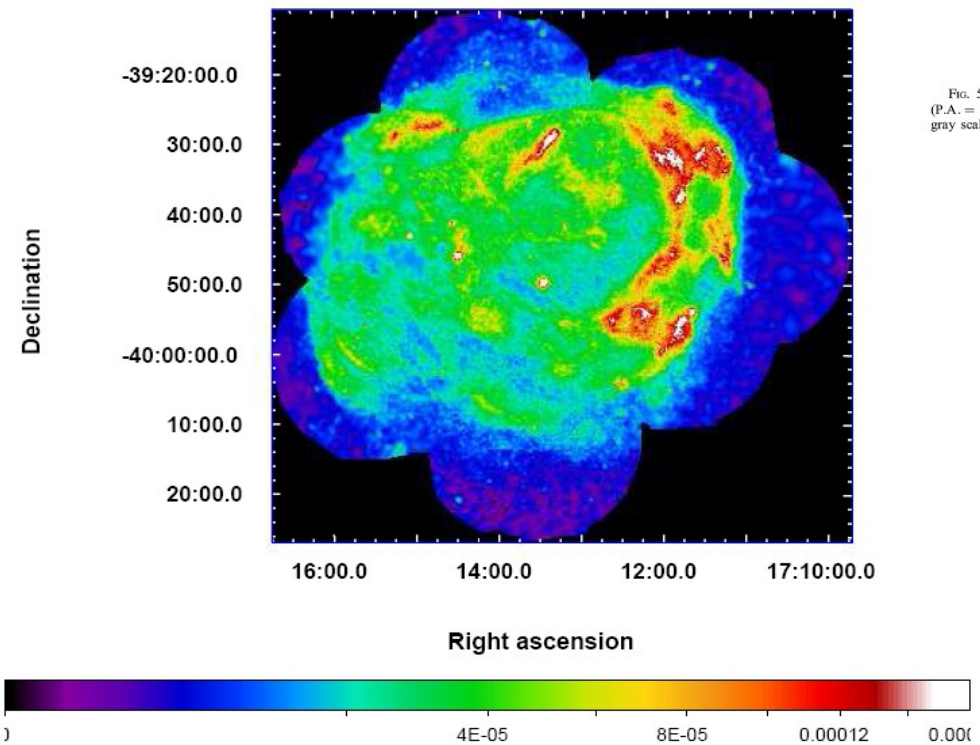


**Fig. 1.** EPIC MOS plus PN image in the 0.5-4.5 keV band. The units are ph/cm$^2$/s/arcmin$^2$ and the scale is square root. The image was adaptively smoothed to a signal-to-noise ratio of 10.

Inner ring of X-ray and radio-emission is probably related with electrons accelerated at the reverse shock.

# Modeling of density distribution around Cas A (Schure et al. 2009, sim. Borkowsky et al. 1996)

Stellar winds of progenitor (sim. SN 1987A, 1993J)

Collision of dense red supergiant and rarefied Wolf-Rayet winds

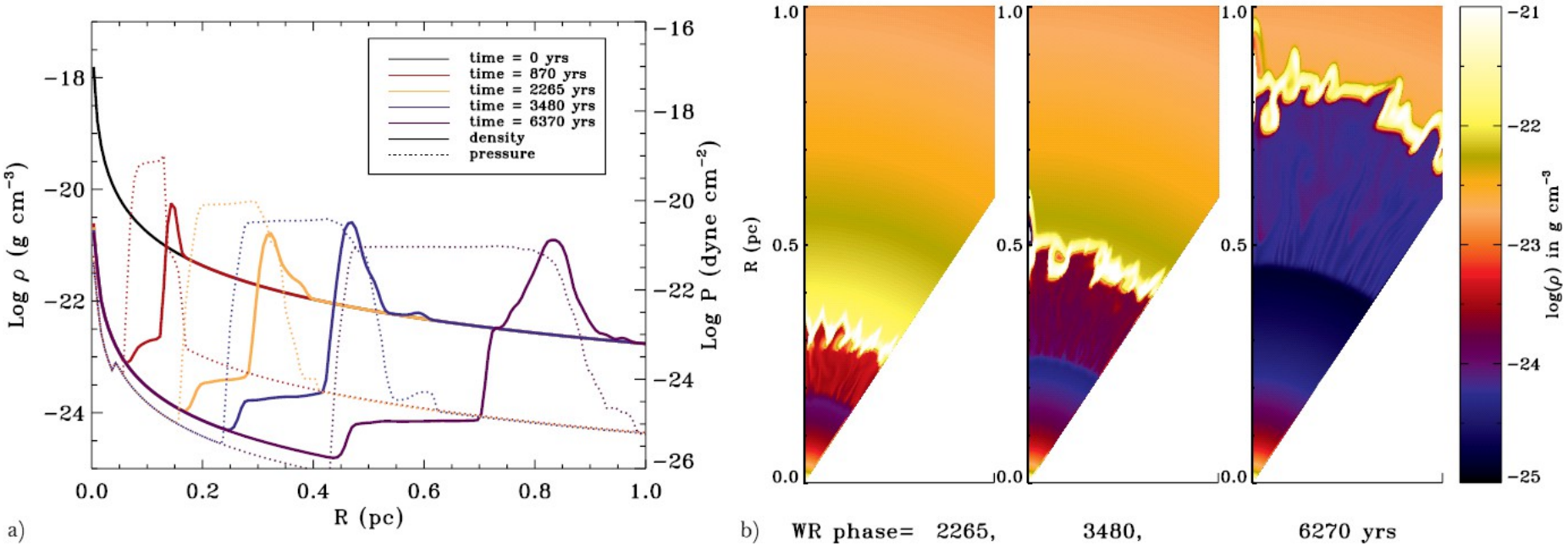


FIG. 2.—(*a*) CSM density (*solid lines*) and pressure (*dotted lines*) due to the RSG and WR winds are shown, for different stages in the evolution. The black solid line shows only the free-streaming RSG wind. For longer WR phases the WR shell broadens and the density contrast increases. The shocks appear smooth due to averaging over the $\pi/4$-angle we used in the 2D simulation. (*b*) CSM density evolution is plotted in 2D, which exemplifies the irregularities in the shell due to the Vishniac thin shell instability. The three panels show the CSM for different durations of the WR phase and correspond to the last three profiles in (*a*). The forward shock is marked by the sudden increase in density and corresponds to the outer boundary of the shell, at a radius of approximately 0.35, 0.5, and 0.9 pc. The contact discontinuity corresponds to the sudden drop in density and the inner boundary of the thin shell. The wind-termination shock is located at around 0.15, 0.25, and 0.45 in the three panels, respectively.

# Diffusion coefficient

$$D=D_B\eta(1+p/P_{f,b})$$

$D_B=\mathrm{v}r_g/3$ - Bohm diffusion coefficient

$\eta=2$

$r_g=pc/qB$ - gyroradius

*At high momenta $p$ $D \sim p^2$, - scattering by small scale random magnetic fields (Dolginov & Toptygin 1967)*

*parameter $P_{f,b}$ was adjusted to reproduce gamma observations*

*The scale of the non-resonant instability depends on the magnetic field. This scale also determines the small-scale scattering of particles. Hence the parameter $P_{f,b}$ may be used to estimate the strength of magnetic field in the medium were the shock propagates.*

# Modeling of Cas A
## (Zirakashvili et al. 2014)

| model | $M_{ej}$ [a] | $k_{ej}$ [b] | $R_f$ [c] | $D$ [d] | $R_s$ [e] | $M_A^f$ [f] | $M_A^b$ [g] | $n_H$ [h] | $E_{SN}$ [i] | $n_{ej}$ [j] | $R_b$ [k] | $R_c$ [l] | $V_f$ [m] | $V_b$ [n] | $V_{be}$ [o] | $B_f$ [p] | $B_b$ [q] |
|---|---|---|---|---|---|---|---|---|---|---|---|---|---|---|---|---|---|
| H1 | 2.0 | 9 | 2.5 | 3.4 | 1.5 | 4.5 | 8 | 0.40 | 1.2 | 0.69 | 1.68 | 2.07 | 5.8 | 0.77 | 4.2 | 1.16 | 0.57 |
| H2 | 2.0 | 9 | 2.5 | 3.4 | 0 | 5 | 5 | 0.36 | 1.2 | 0.67 | 1.82 | 1.90 | 6.0 | 4.0 | 1.4 | 1.0 | 0.27 |
| L1 | 2.0 | 9 | 2.5 | 3.4 | 0 | 10 | 10 | 1.0 | 2.0 | 0.30 | 1.64 | 1.74 | 5.7 | 3.1 | 1.8 | 0.78 | 0.12 |

[a] mass of ejecta, solar masses
[b] power-law index of ejecta density distribution
[c] forward shock radius, pc
[d] distance to SNR, kpc
[e] RSG shell radius, pc
[f] parameter of magnetic amplification at the forward shock
[g] parameter of magnetic amplification at the reverse shock
[h] undisturbed hydrogen number density at the forward shock position, $cm^{-3}$
[i] explosion energy, $10^{51}$ erg
[j] number density of unshocked ejecta, nucleons $cm^{-3}$
[k] reverse shock radius, pc
[l] radius of the contact discontinuity, pc
[m] forward shock speed, $10^3$ km $s^{-1}$
[n] reverse shock speed in the laboratory frame, $10^3$ km $s^{-1}$
[o] reverse shock speed in the ejecta frame, $10^3$ km $s^{-1}$
[p] magnetic field just downstream of the forward shock, mG
[q] magnetic field just downstream of the reverse shock, mG

# Numerical results for Cas A
# (Zirakashvili et al. 2014)

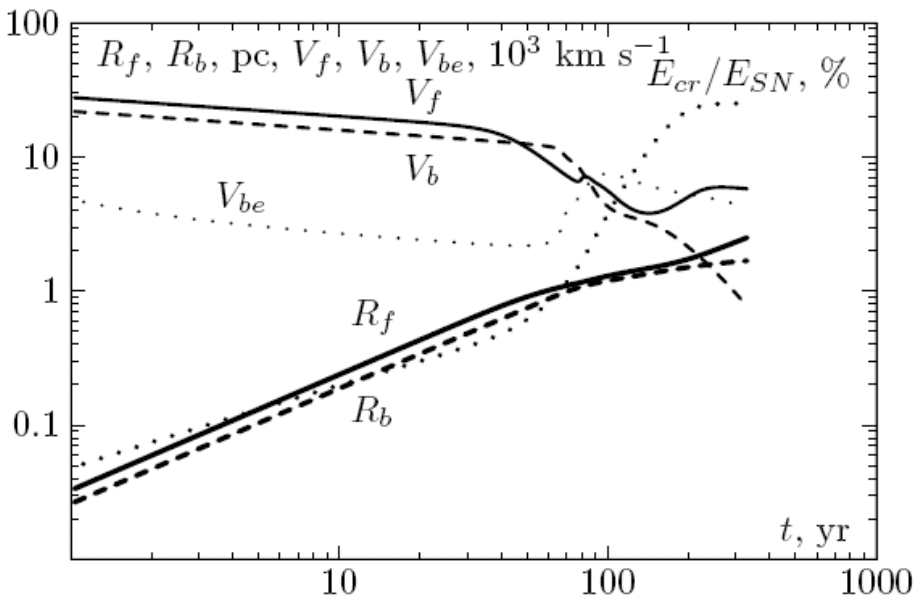


Fig. 1.— Time dependencies of parameters characterizing the forward and reverse shocks: the forward shock radius $R_f$ (thick solid line), the reverse shock radius $R_b$ (thick dashed line), the forward shock speed $V_f$ (thin solid line), the reverse shock speed $V_b$ (thin dashed line), the reverse shock speed in the ejecta frame $V_{be}$ (thin dotted line). The ratio of the energy released in cosmic rays to the total energy of the supernova explosion $E_{cr}/E_{SN}$ (dotted line) is also shown.

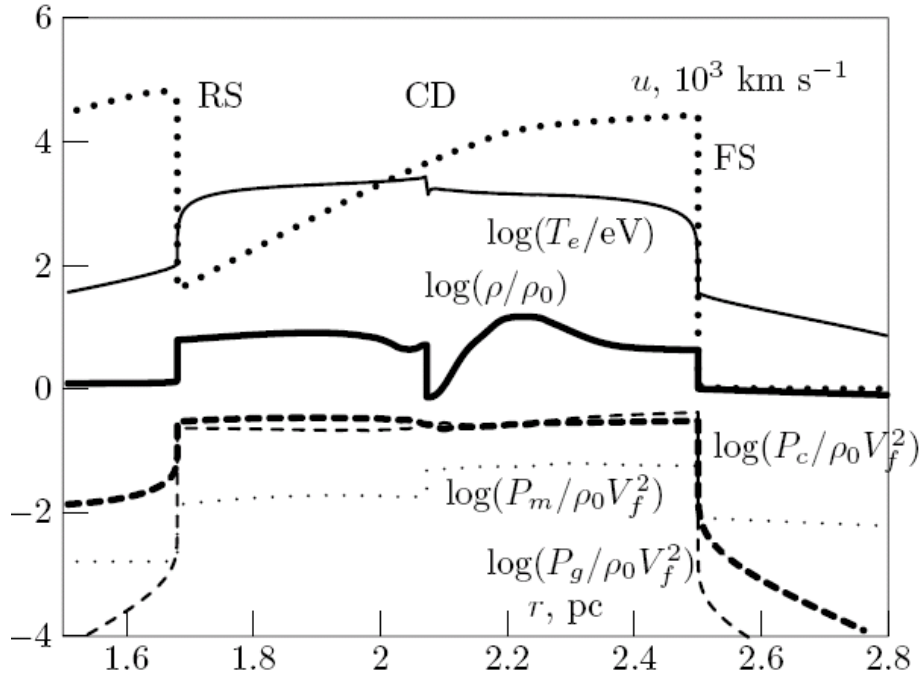


Fig. 2.— Radial dependencies of the gas density (thick solid line), the gas velocity (thick dotted line), the CR pressure (thick dashed line), the gas pressure (dashed line), the magnetic pressure (dotted line) and the electron temperature (solid line) at the epoch $t = 330$ yr. In the same figure the positions of the forward and reverse shocks, (FS and RS, respectively) as well as of the contact discontinuity (CD) are shown.

# Spectra of particles at FS and RS

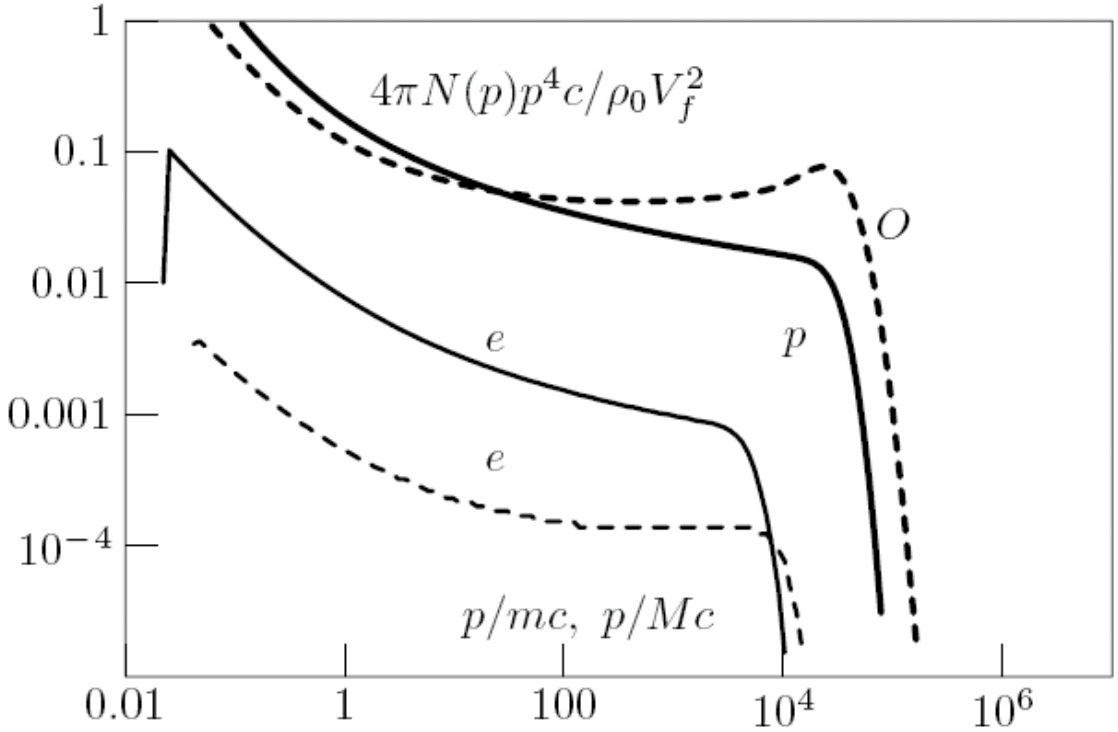


Fig. 3.— The energy distributions of protons at the forward shock (thick line), of oxygen ions at reverse shock (thick dashed line), of electrons at the forward shock (multiplied to the factor of $10^2$, thin lines) and of electrons at the reverse shock (thin dashed line) calculated for the model H1 at the epoch $t = 330$ yr. Particle momenta are normalized to the proton mass $m$ and the mass of oxygen ion $M$. The oxygen spectrum is normalized to the nucleon number density.

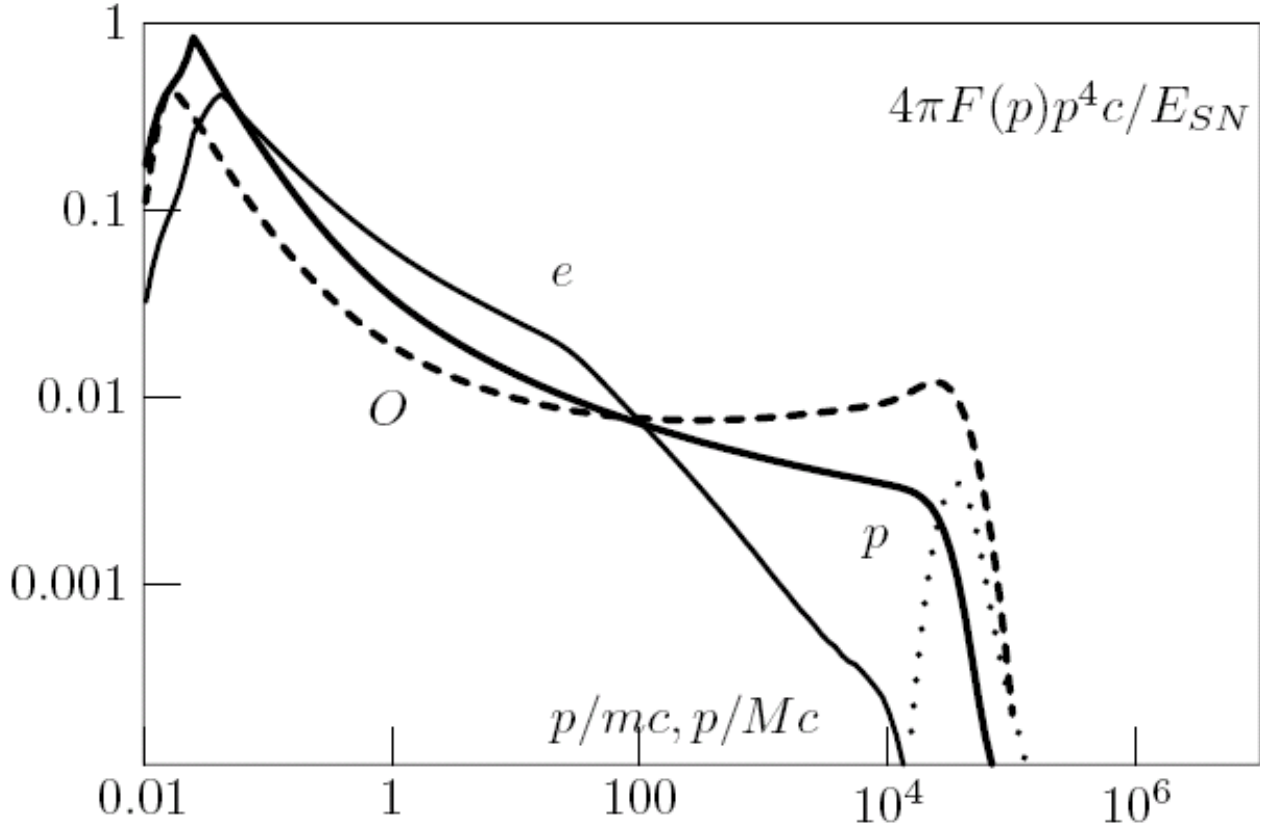


Fig. 4.— Spatially integrated spectra of accelerated protons (solid line), oxygen ions (dashed line) and electrons multiplied to $10^3$ (thin solid line) at $t = 330$ yr obtained in the model H1. Spectrum of run-away protons which have left the remnant is also shown (dotted line).

# Volume-integrated spectra

$E_{max}$=80 TeV in hadronic model H1

# Spectra of electromagnetic radiation of Cas A (hadronic model H1, RSG shell at 1.5 pc)

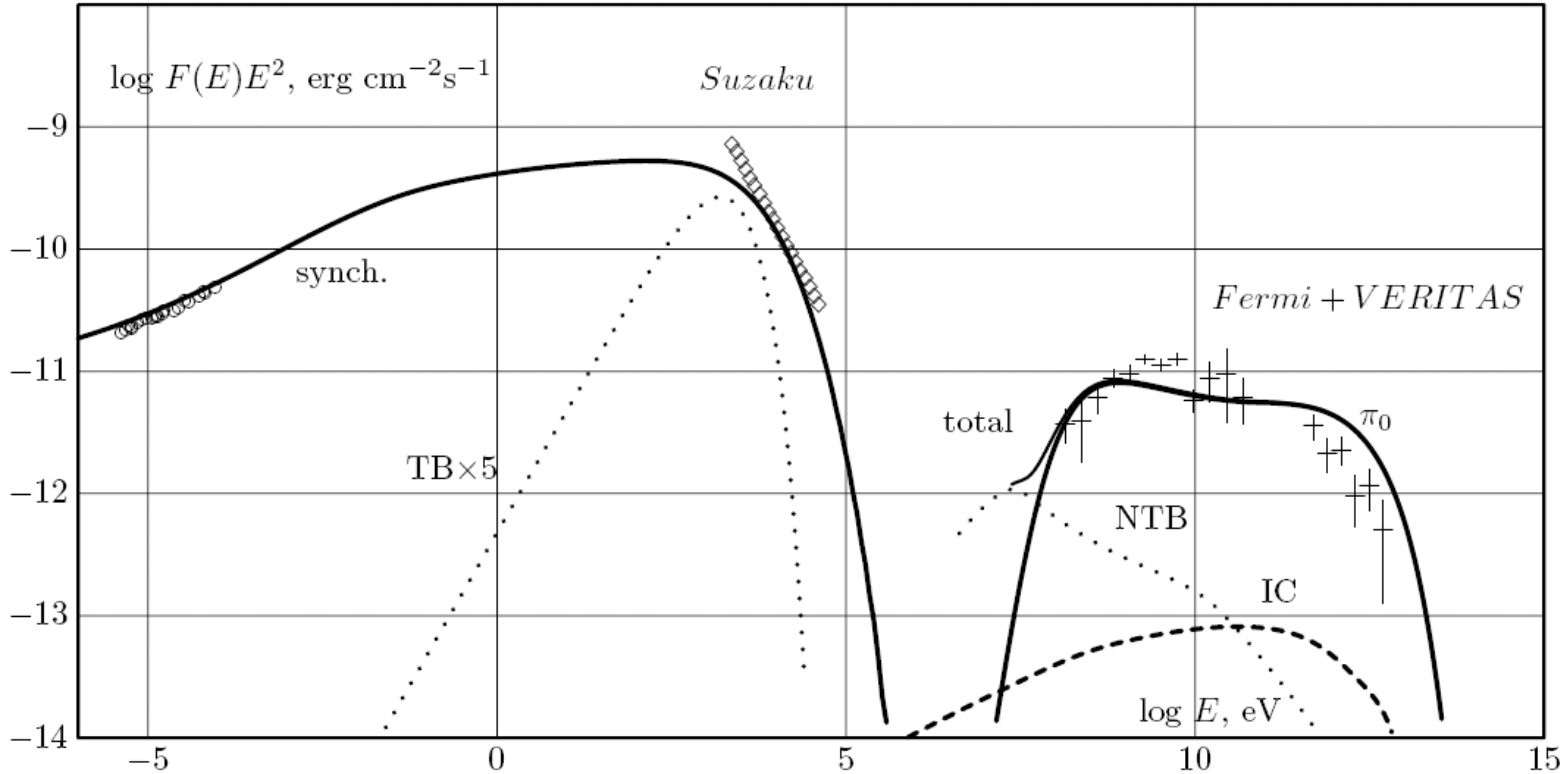


RS dominates in X-rays and gives a significant contribution in gamma-rays and radio

Fig. 6.— The broad-band spectral energy distribution of nonthermal radiation of Cas A calculated within the hadronic model H1. The following radiation processes are taken into account: synchrotron radiation of accelerated electrons (solid curve on the left), IC emission (dashed line), gamma-ray emission from pion decay (solid line on the right), thermal bremsstrahlung (dotted line on the left), nonthermal bremsstrahlung (dotted line on the right). Experimental data in gamma-ray (Fermi LAT, present work); VERITAS, Acciari et al. 2010, data with error-bars) and radio-bands (Baars 1977, circles), as well as the power-law approximation of Suzaku X-ray data (Maeda et al. 2009, diamonds) from the whole remnant are also shown.

# Old SNRs (T>$10^4$ yr) in the dense medium

(Ackermann et al. 2013)

$n_H > 1\ cm^{-3}$

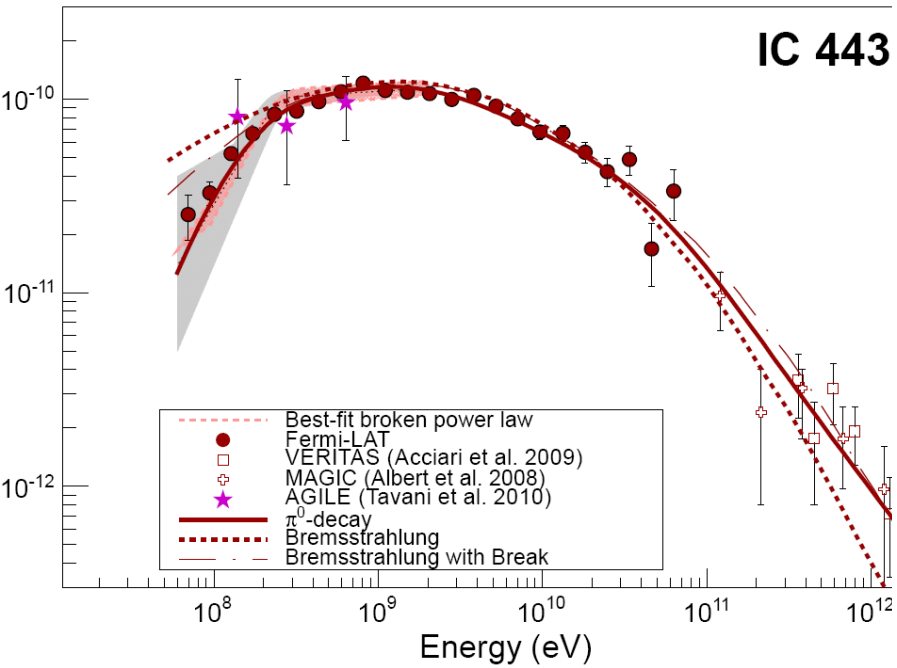


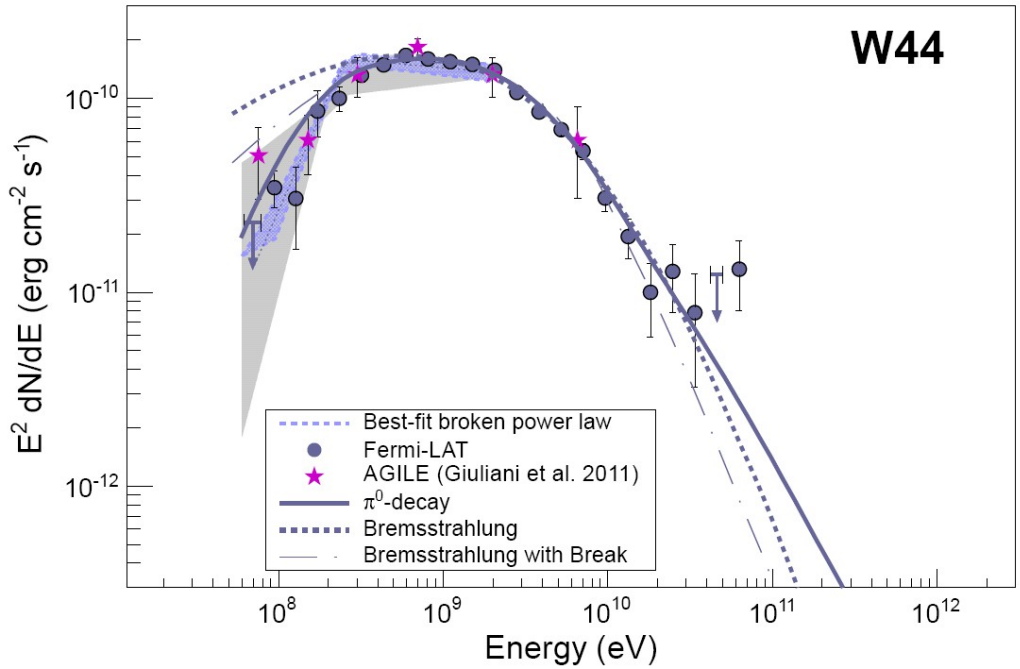


Old SNRs show gamma-ray spectra with steeper parts or cut-offs. TeV protons are not accelerated at present.

$E_{max}$ ~100 GeV in IC443 and $E_{max}$ ~10 GeV in W44. Probably because of neutral damping of MHD waves generated by accelerated particles.

The spectral shape at E<1 GeV favors a hadronic origin of gamma-emission.

# IC443 Radio-optical image (Castelletti, 2011)

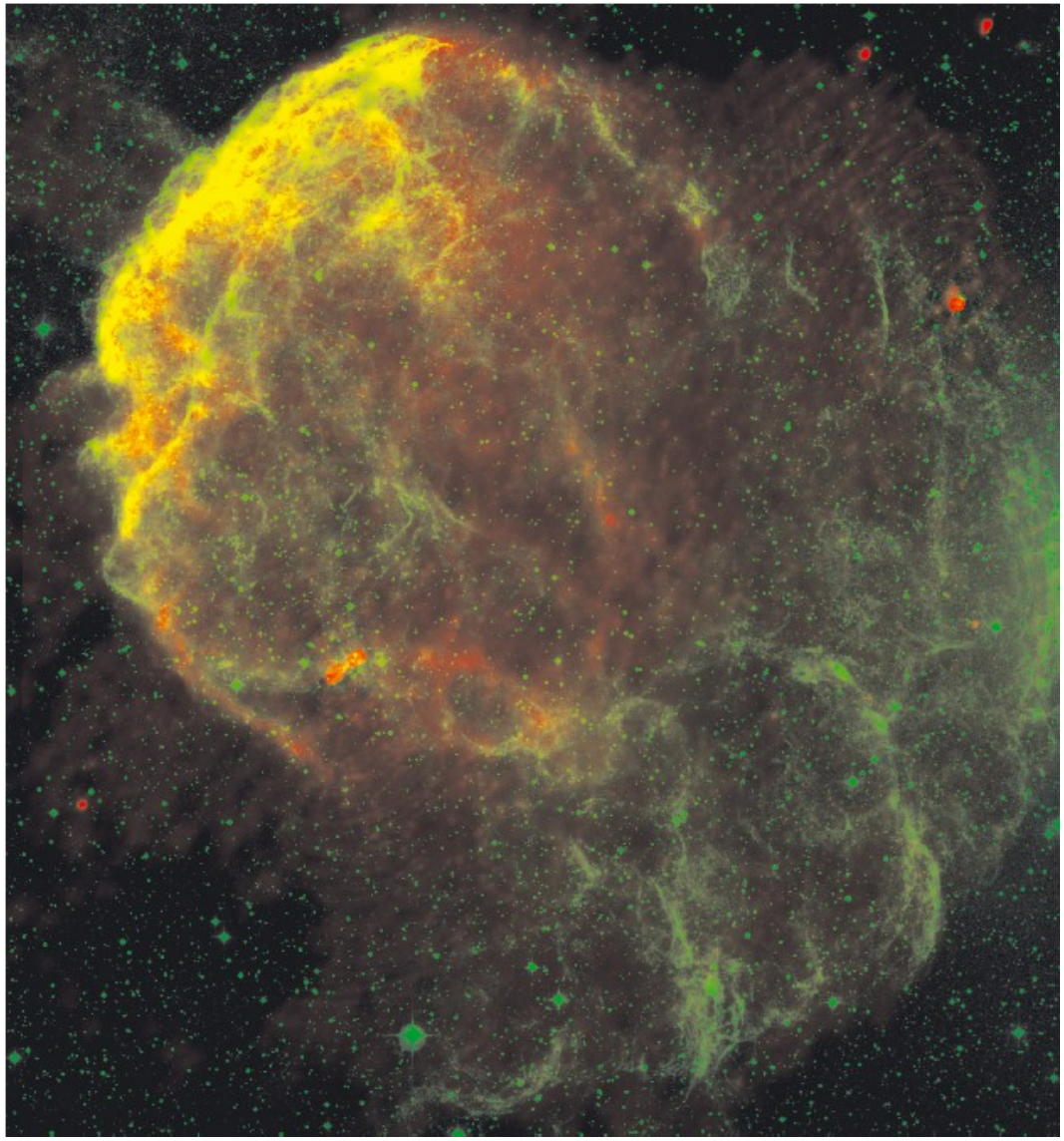

SNR is at radiative stage (optical filaments)

# IC443 image of Veritas

(Humensky 2015)

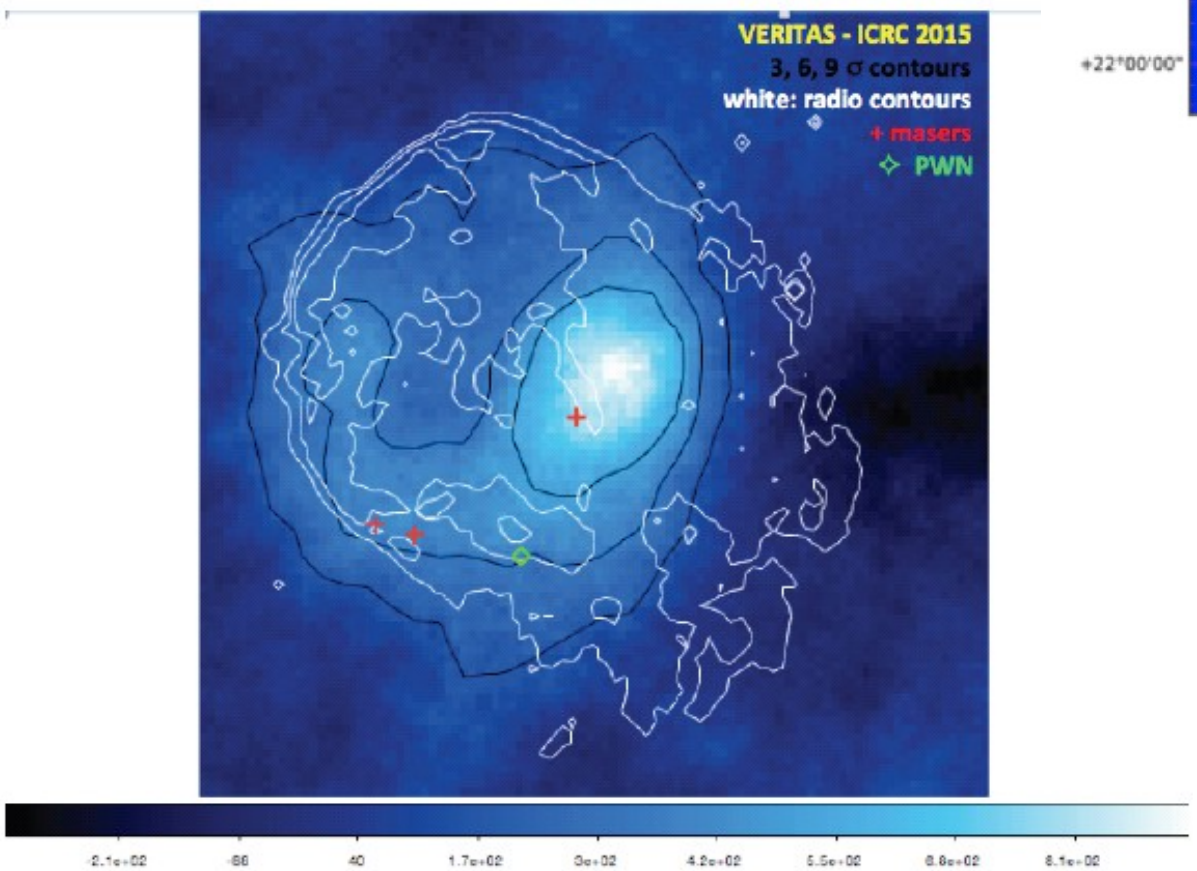


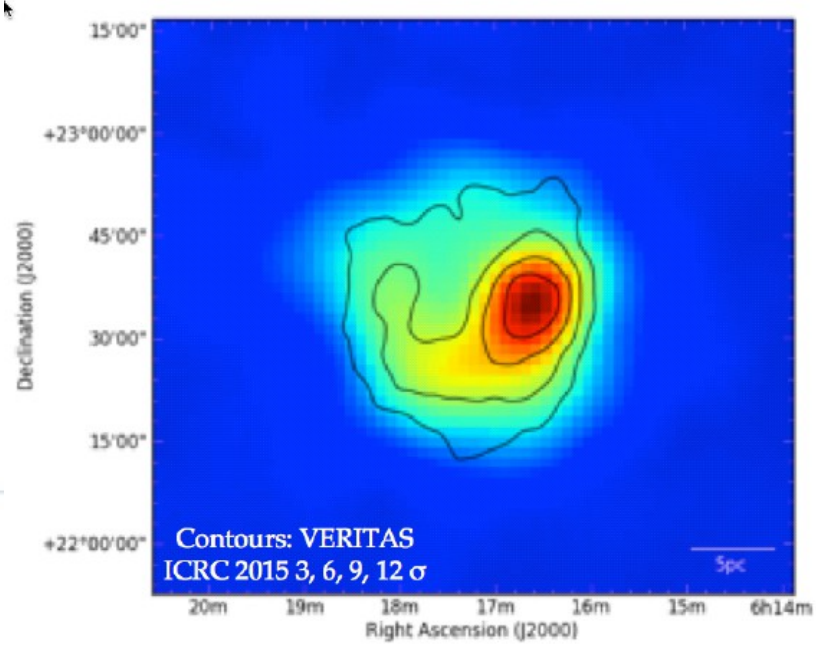


Fermi LAT counts map

Probably high energy multi-TeV protons accelerated earlier are still confined in the SNR shell.

# Fermi gamma ray image of W28 (Hanabata et al. 2014)

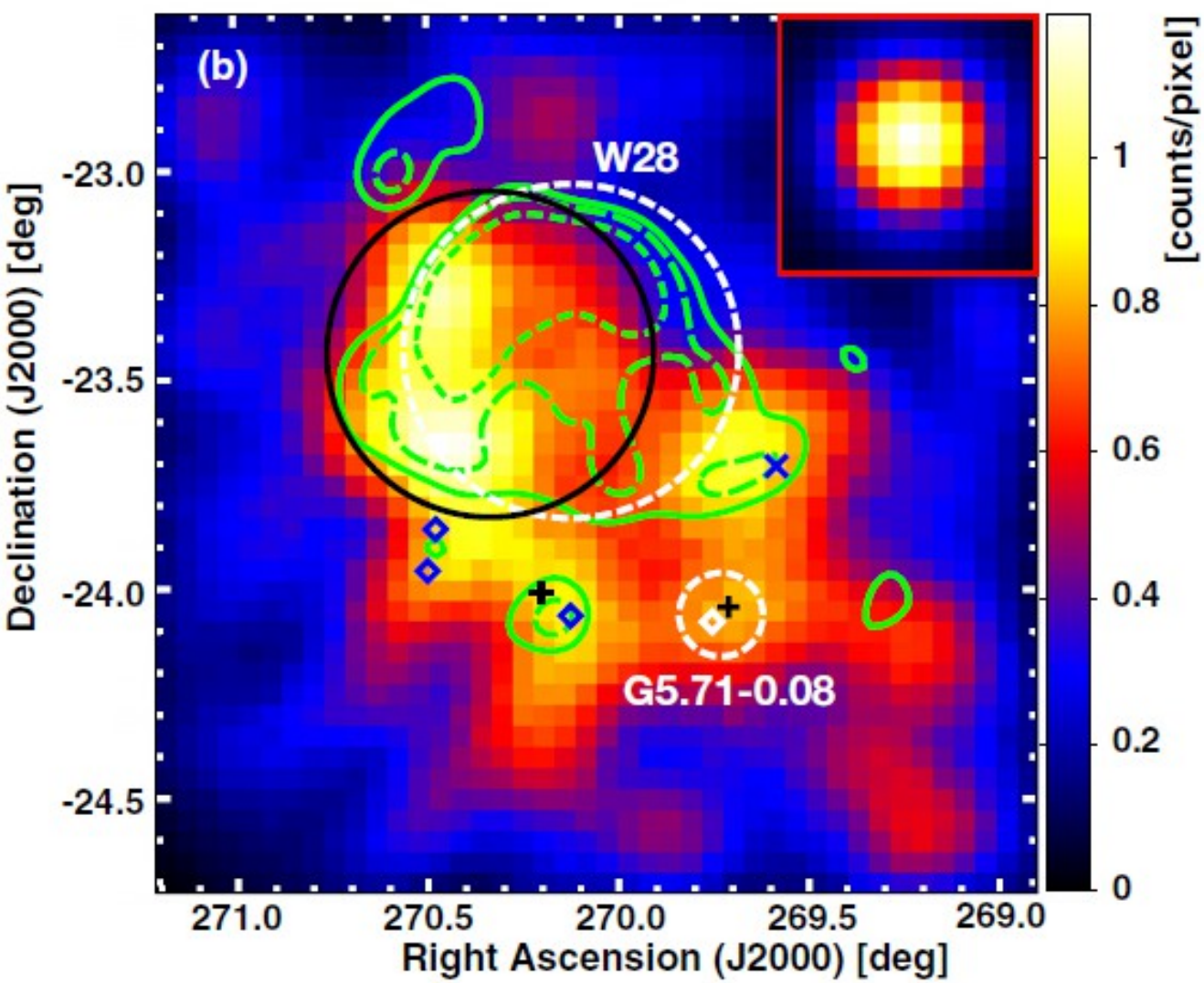


T

# Equations for gas and wave pressure (radiative cooling and wave damping are included )

$$\frac{\partial P_g}{\partial t} + u\frac{\partial P_g}{\partial r} + \frac{\gamma_g P_g}{r^2}\frac{\partial r^2 u}{\partial r} =$$

$$V_{Ar} = V_A/\sqrt{3}$$

$$-(\gamma_g - 1)\left(\Lambda(T)n^2 - 2\Gamma_n\frac{P_m}{\gamma_m - 1} + V_{Ar}(1 - h_m)\frac{\partial P_c}{\partial r}\right)$$

$$\frac{\partial P_m}{\partial t} + (u + V_{Ar})\frac{\partial P_m}{\partial r} + \frac{P_m}{r^2}\frac{\partial r^2(\gamma_m u + V_{Ar})}{\partial r} =$$

$$-h_m(\gamma_m - 1)V_{Ar}\frac{\partial P_c}{\partial r} - 2\Gamma_n P_m$$

$h_m$=1 at $P_m$<10$P_{m0}$ and $h_m$=0.5 at $P_m$>10$P_{m0}$

$D=D_B(P_{m0}+P_m)/P_m$

Upstream of the shock

Bohm diffusion $D=D_B$ , $\Gamma_n=0$ and $V_A=0$ in downstream region

# Modeling of DSA in old remnants (Zirakashvili & Ptuskin 2017)

TABLE I: Physical parameters of SNRs W28, W44 and IC443

| | $d$ | $R_f$ | $E_{SN}$ | $M_{ej}$ | $n_H$ | $n_n$ | $K_{ep}$ | $T$ | $V_f$ | $B_f$ |
|---|---|---|---|---|---|---|---|---|---|---|
| | kpc | pc | $10^{51}$erg | $M_\odot$ | $cm^{-3}$ | $cm^{-3}$ | | kyr | km/s | $\mu$G |
| W28 | 1.9 | 13.4 | 1.3 | 6.8 | 4.0 | 0.2 | 0.008 | 37 | 121 | 79 |
| W44 | 2.8 | 12.4 | 1.6 | 7.1 | 6.0 | 0.3 | 0.006 | 33 | 130 | 102 |
| IC443 | 1.5 | 9.9 | 0.9 | 6.3 | 3.0 | 0.15 | 0.008 | 17 | 196 | 110 |

Probably SNRs of type IIP supernova

W28 profiles at T=37 kyrs

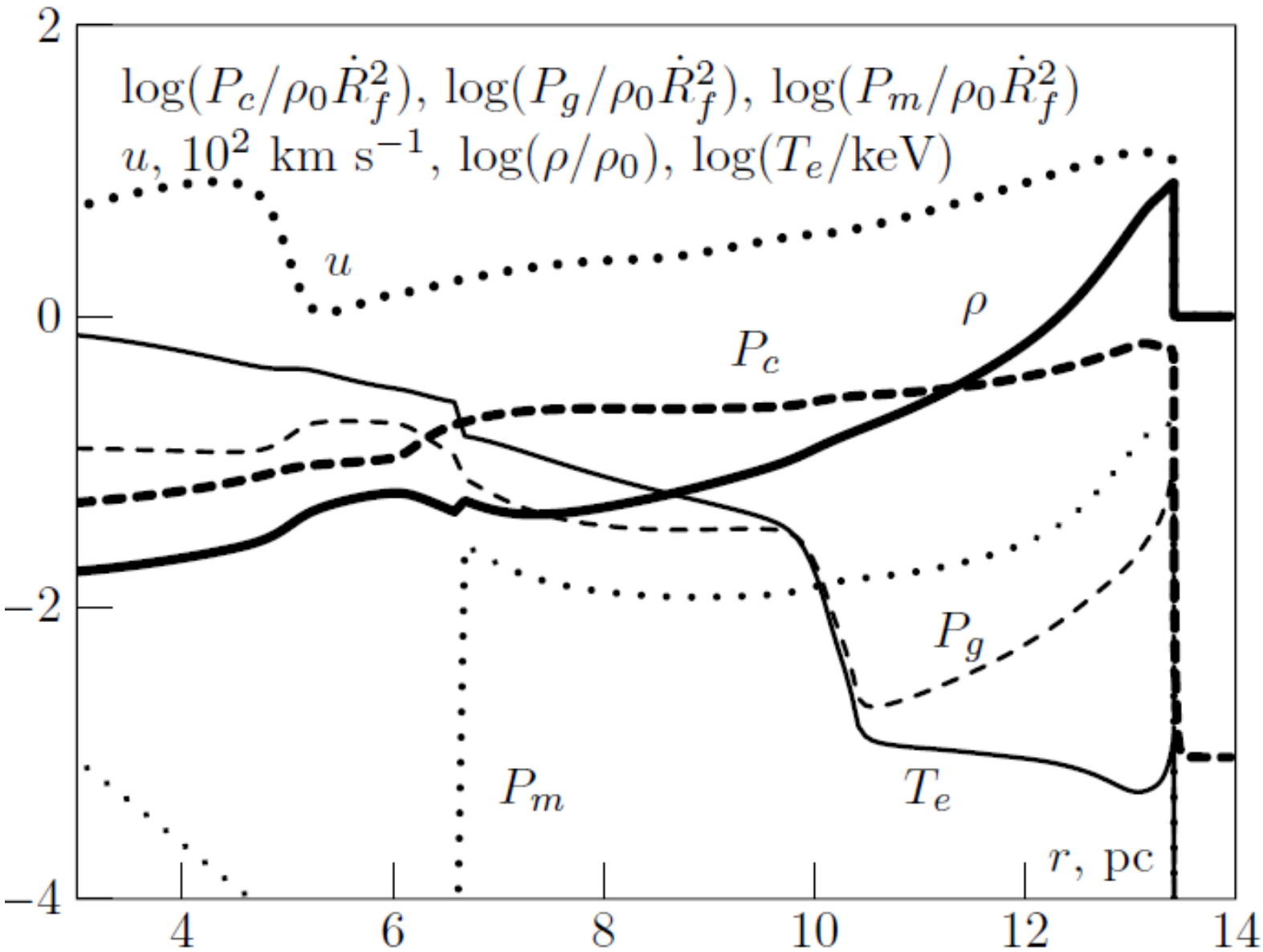

# Spectra of particles at T=37 kyrs

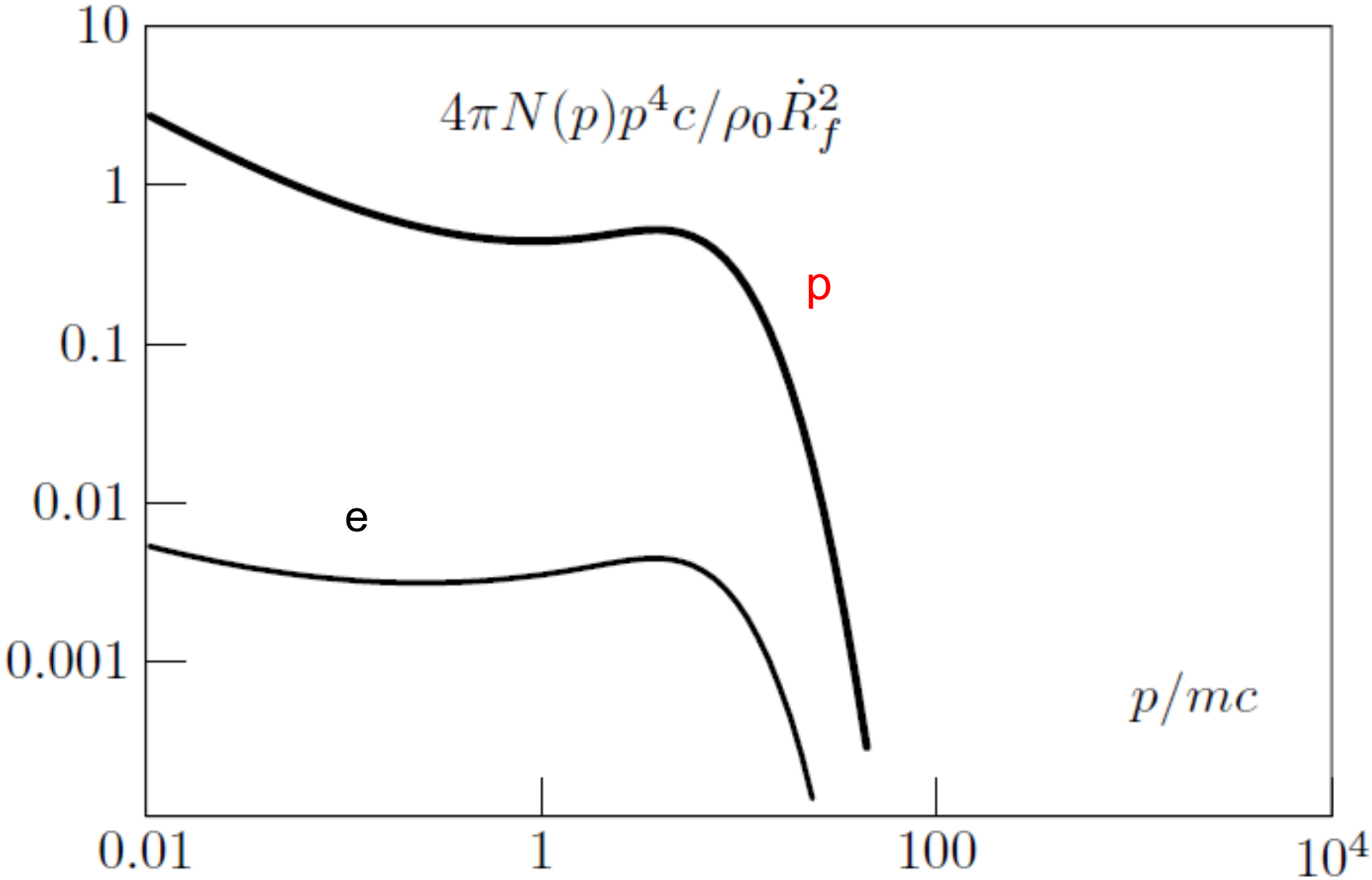

# Spectra of particles produced in W28

80 % of energy is transferred to CRs

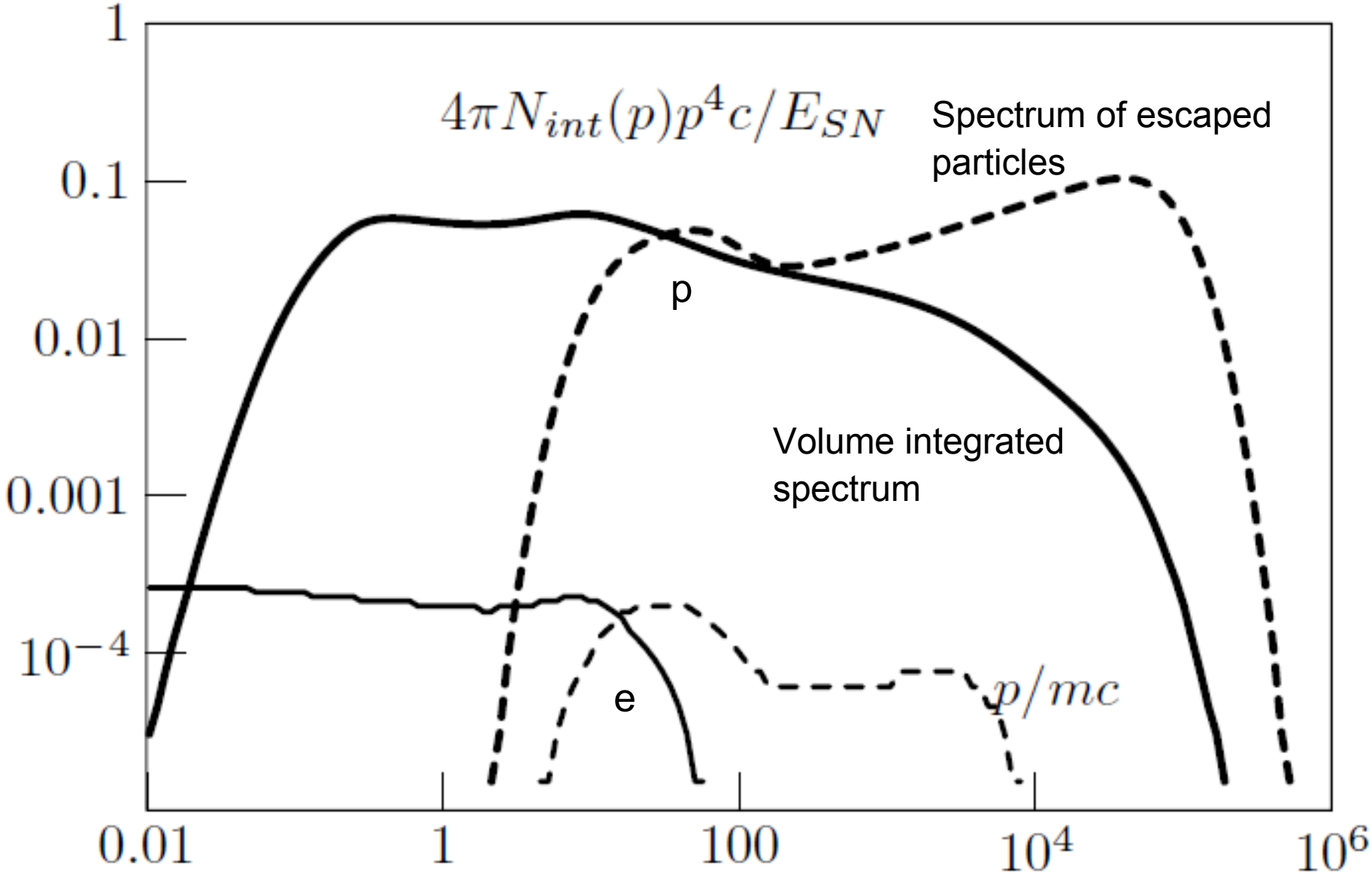

# Spectra of W28

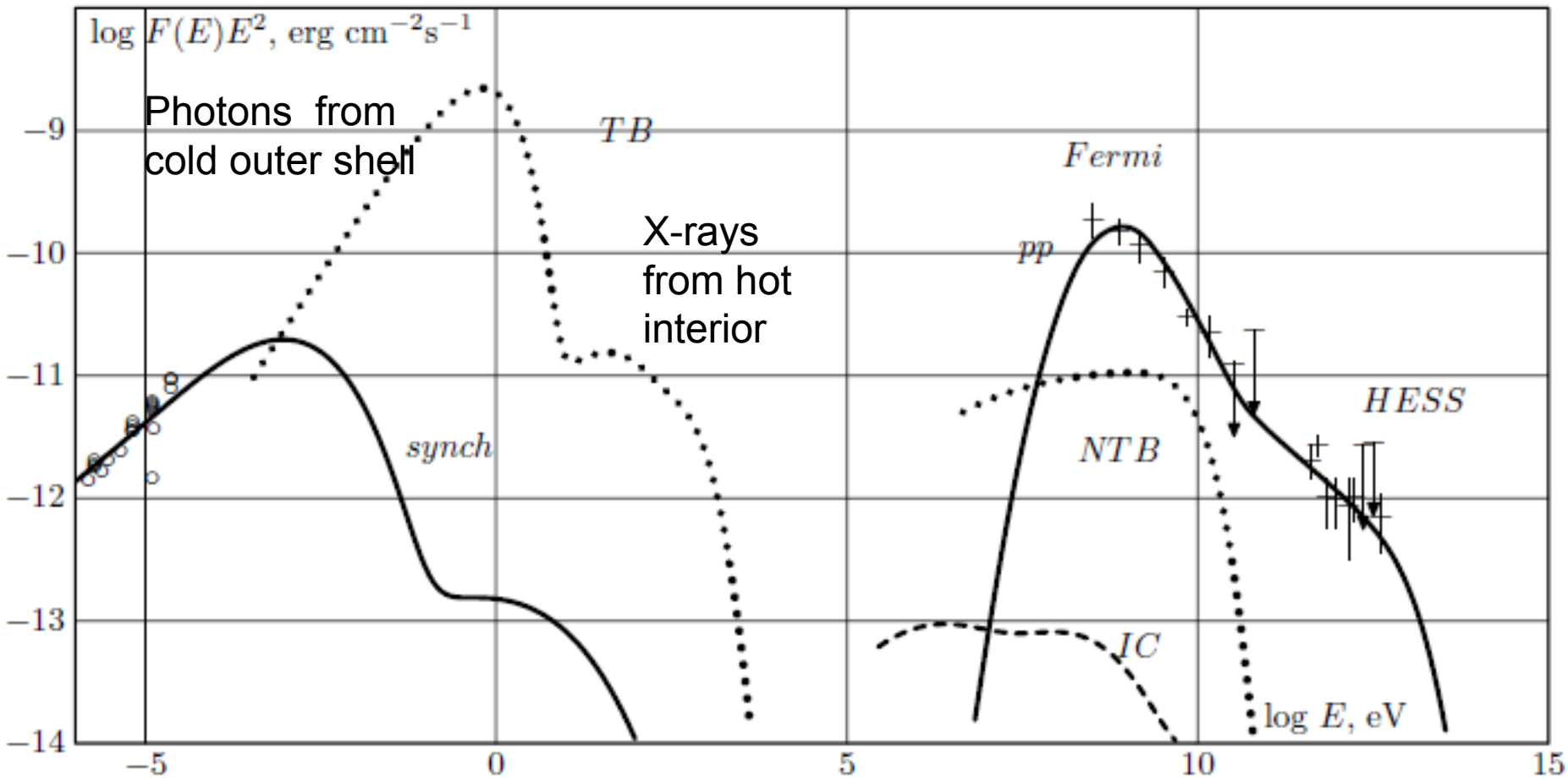


d=1.9 kpc, $E_{SN}$=1.3·$10^{51}$ erg, $M_{ej}$=6.8 $M_{sol}$, t=37 kyr, $n_H$=4.0 $cm^{-3}$, $n_n$=0.2 $cm^{-3}$

$V_f$=120 km/s, $B_f$=8 $10^{-5}$ G, $K_{ep}$=0.008

# Spectra of W44

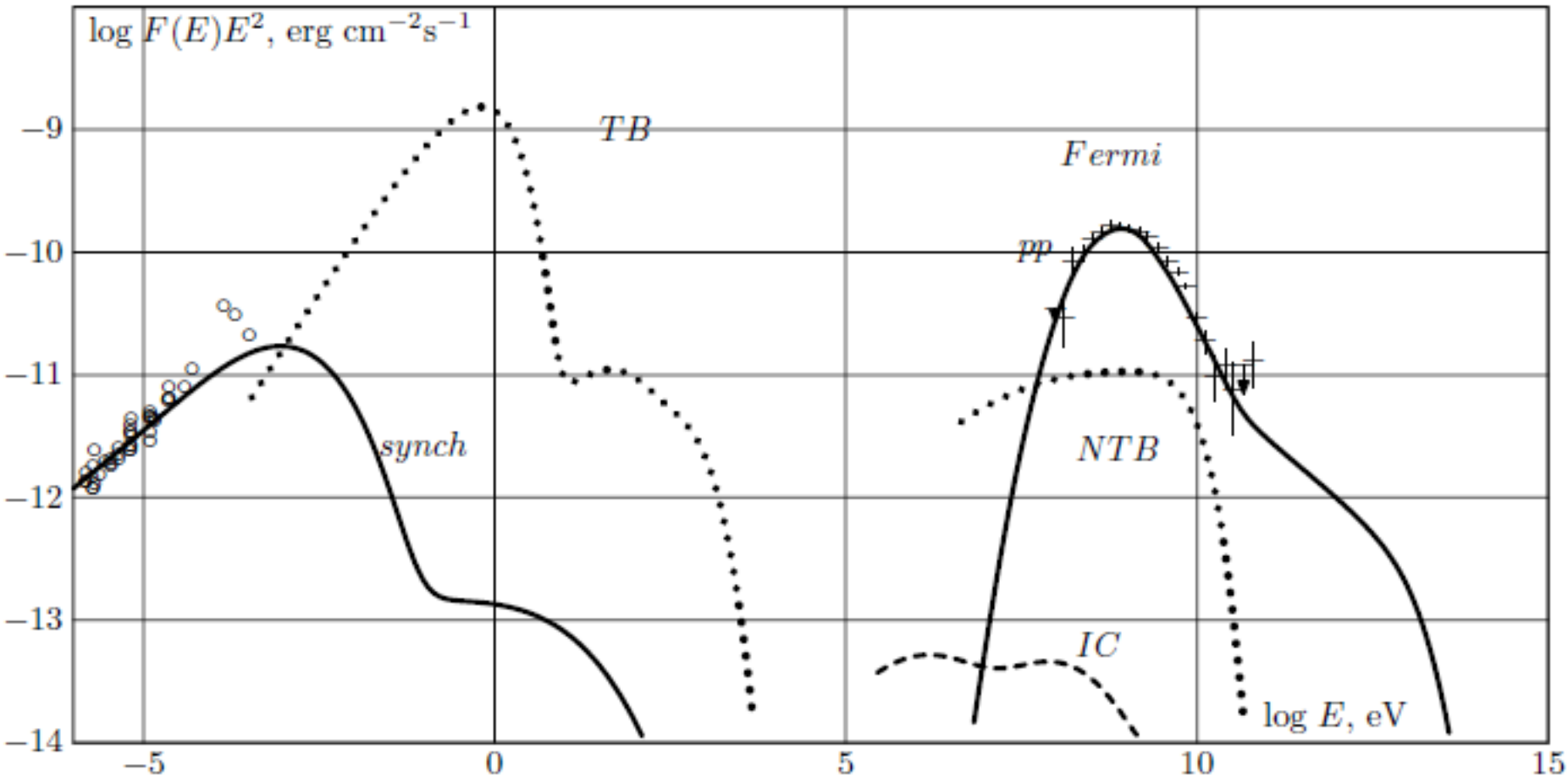


d=2.8 kpc, $E_{SN}=1.6\cdot10^{51}$ erg, $M_{ej}=7.1\ M_{sol}$, t=33 kyr, $n_H=6.0\ cm^{-3}$, $n_n=0.3\ cm^{-3}$

$V_f=130$ km/s, $B_f=10^{-4}$ G, $K_{ep}=0.006$

# Spectra of IC443

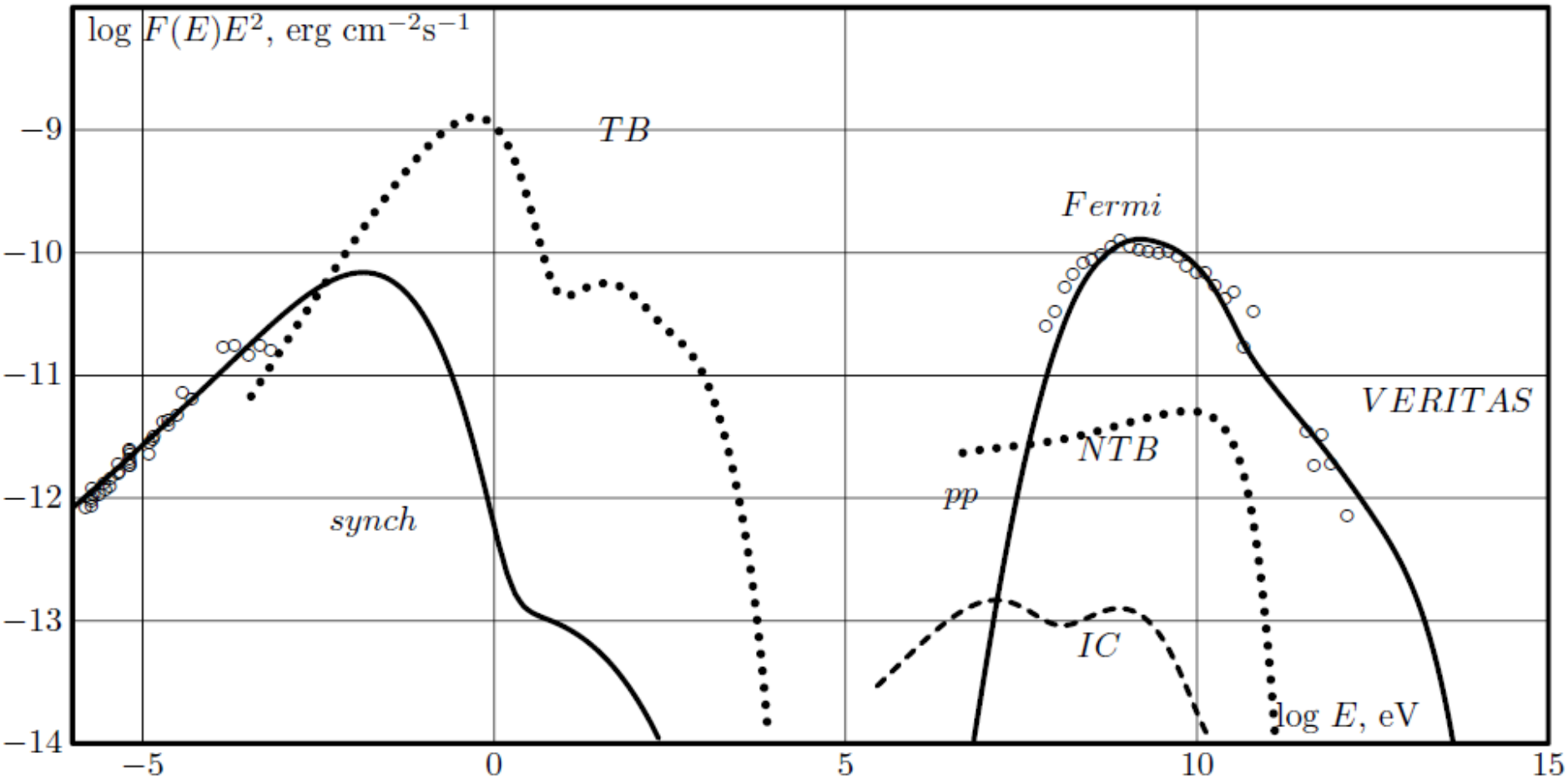


$E_{SN}$=0.9·10$^{51}$ erg, $M_{ej}$=6.3 $M_{sol}$, t=17 kyr, $n_H$=3.0 cm$^{-3}$, $n_n$=0.15 cm$^{-2}$

$V_f$=200 km/s, $B_f$=1.1 10$^{-4}$ G,

# Is the number of such SNRs enough for origin of galactic CRs?

YES

$L_{SNR} \sim E_{SN}/T \sim 10^{39}$ erg/s

100 such SNRs can provide Galactic CR power

Fermi LAT detected about 20 brightest and closest SNRs of this kind with gamma ray energy flux
$F>10^{-11}$ erg $cm^{-2}$ $s^{-1}$

But modest maximum energies close to 100 TeV

# “Knee” energies for SNRs in different circumstellar media (Bohm diffusion in the amplified magnetic field - optimistic estimate )

Uniform medium

SNRs of Ia supernovae

$$E_{\text{knee}} = 3Z\,\text{PeV}\left(\frac{E_{SN}}{10^{51}\,\text{erg}}\right)\left(\frac{M_{ej}}{M_{\text{solar}}}\right)^{-2/3} n_H^{1/6}$$

Stellar wind

$$E_{\text{knee}} = 80Z\,\text{PeV}\left(\frac{E_{SN}}{10^{52}\,\text{erg}}\right)\left(\frac{M_{ej}}{10M_{\text{solar}}}\right)^{-1}\left(\frac{\dot{M}}{10^{-2}M_{\text{solar}}\,\text{yr}^{-1}}\right)^{1/2}\left(\frac{u_w}{100\,\text{km/s}}\right)^{-1/2}$$

SNRs of IIP, IIb, IIn supernovae

quasi-parallel shocks, nonresonant instability (Bell 2004)

10 times lower energies

higher for oblique shocks

# Eta Carinae - progenitor of IIn supernova in future

Very dense circumstellar medium results in high maximum energies and in effective production of gamma rays and neutrinos

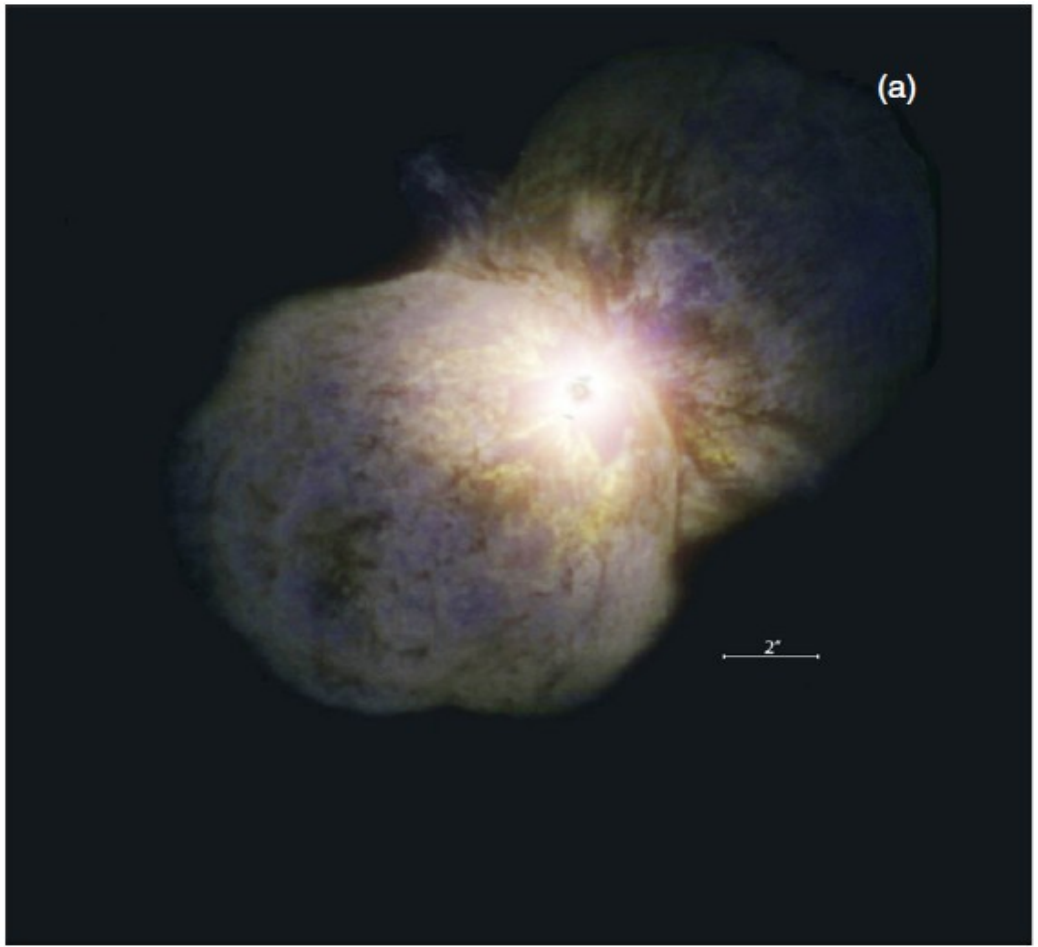


Homunculus nebula

~1 solar mass

appeared after Great eruption in 1844

# high energy neutrinos of cosmic origin

**IceCube neutrino detector**

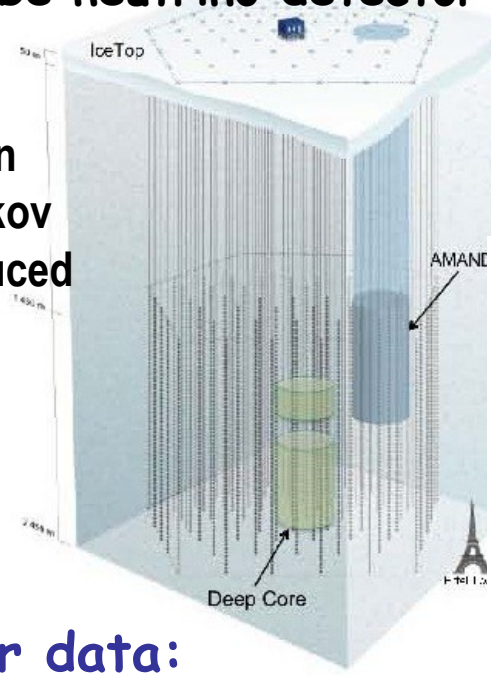


registration of Cherenkov light produced in ice by charged secondary particles

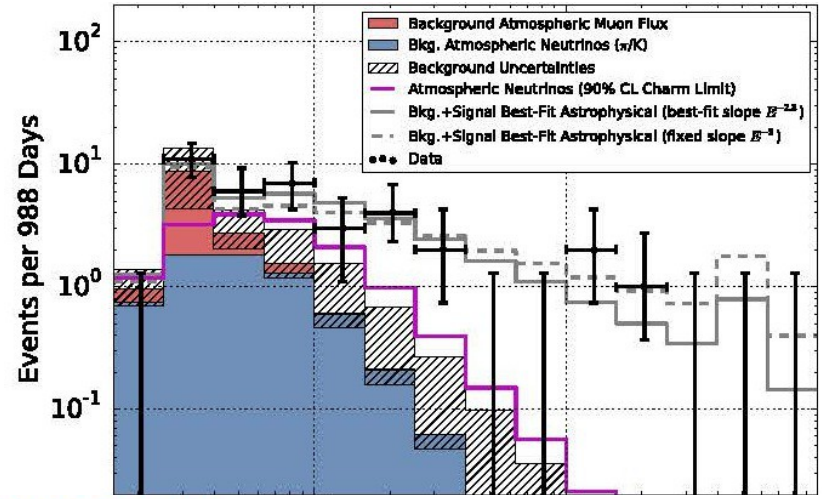


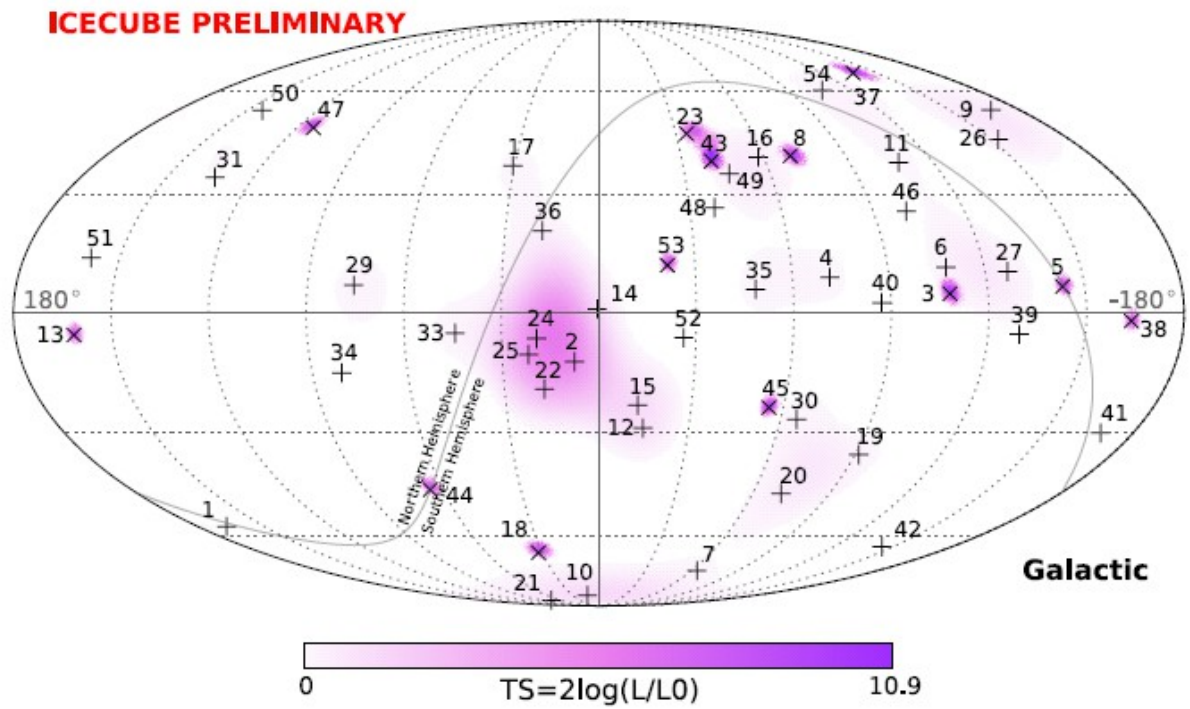


**3-year data: excess of 37 neutrinos above background (>5.7 sigma) at $3.10^{13}$ to $2.10^{15}$ eV**

4th year - 17 neutrinos

$$E_\nu^2\left(dN/dE_\nu\right)=(0.95\pm0.3)\times10^{-8}\ \mathrm{GeV\ cm^{-2}\ s^{-1}\ sr^{-1}}$$

Aartsen et al. 2014

IceCube Coll. 2015

# Evolution of supernova remnant during 30 years after IIn supernova explosion (Zirakashvili & Ptuskin 2016)

25% of explosion energy goes into accelerated particles

$E_{SN}=10^{52}$ erg

$M_{ej}=10\ M_S$

Mass loss rate

$dM/dt=10^{-2}$

$M_S$ per year

Stellar wind speed

$u_w=100$ km/s

parameters from

Moriya et al.

2014

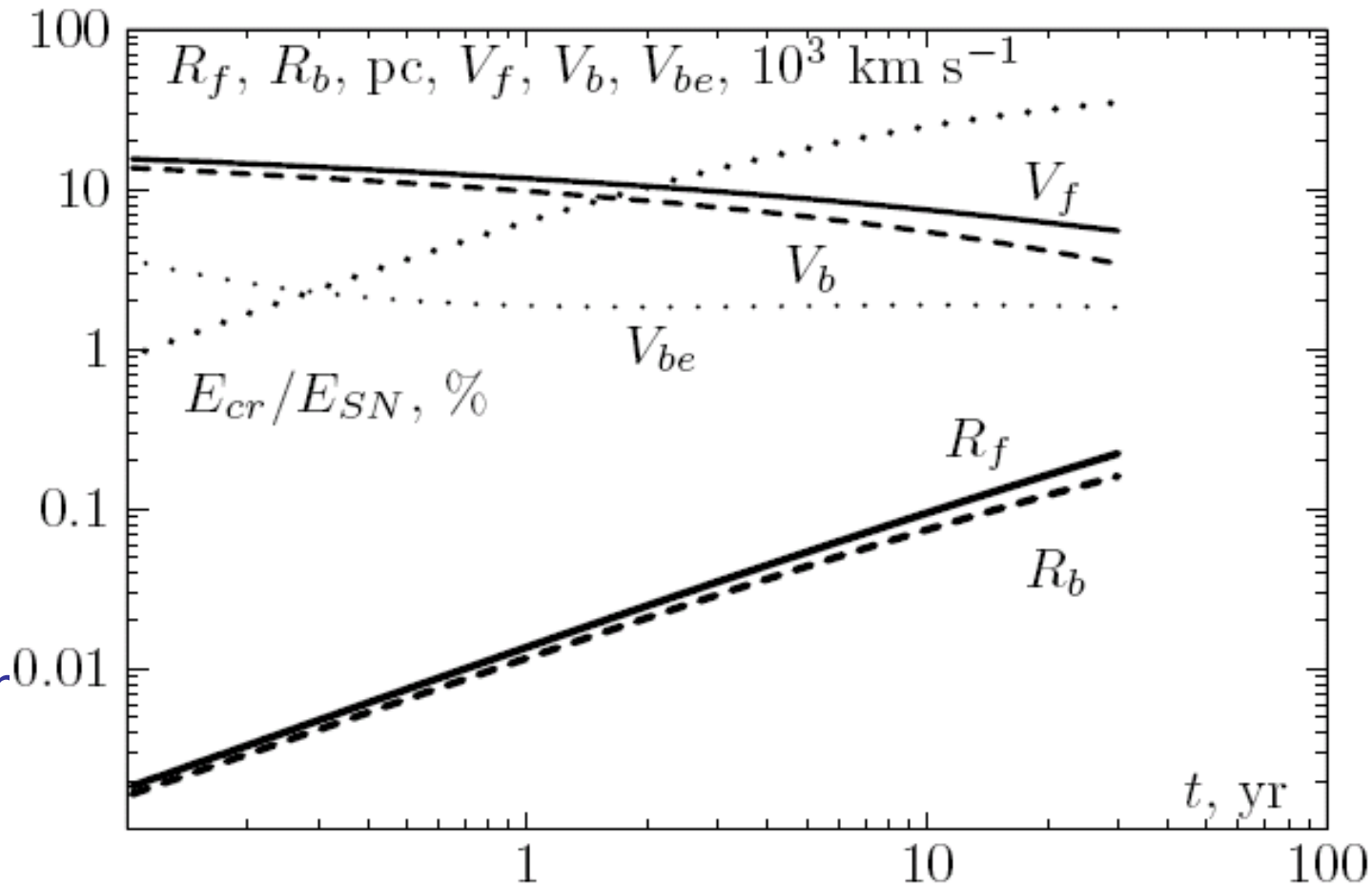

# Spectra of accelerated particles and pp – neutrinos produced during 30 years after IIn supernova explosion

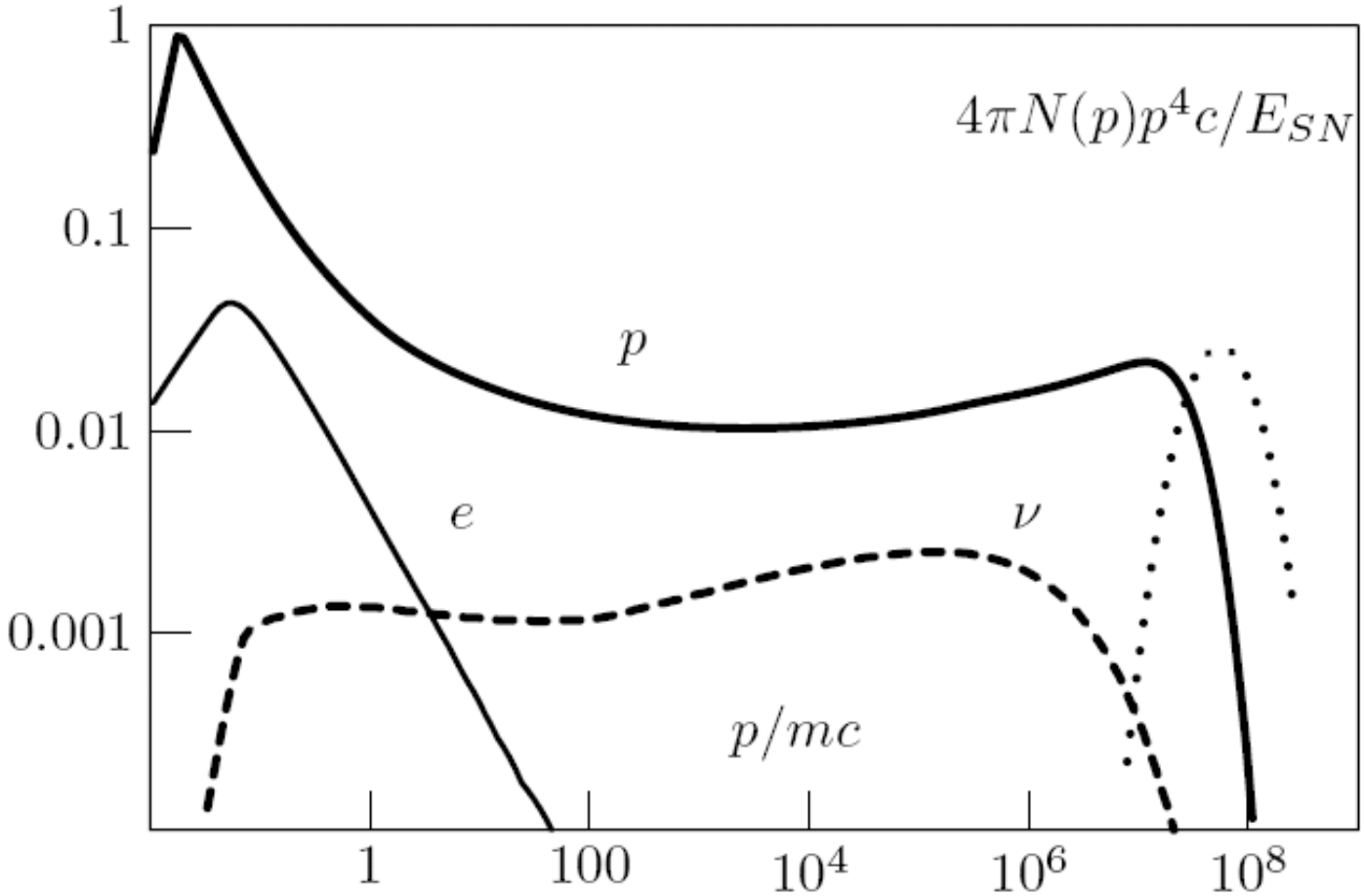

# Background spectrum of astrophysical neutrinos

$$F(E) = cH_0^{-1} \int_E^{E(1+z_{\max})} \frac{dE'}{E} \left( \frac{E'}{E} \right)^m \frac{q(E')}{\sqrt{\Omega_\Lambda + \Omega_M E'^3 / E^3}}$$

*m* describes evolution of sources $q \sim (1+z)^m$

Dependence of supernova rate

and star formation rate on z

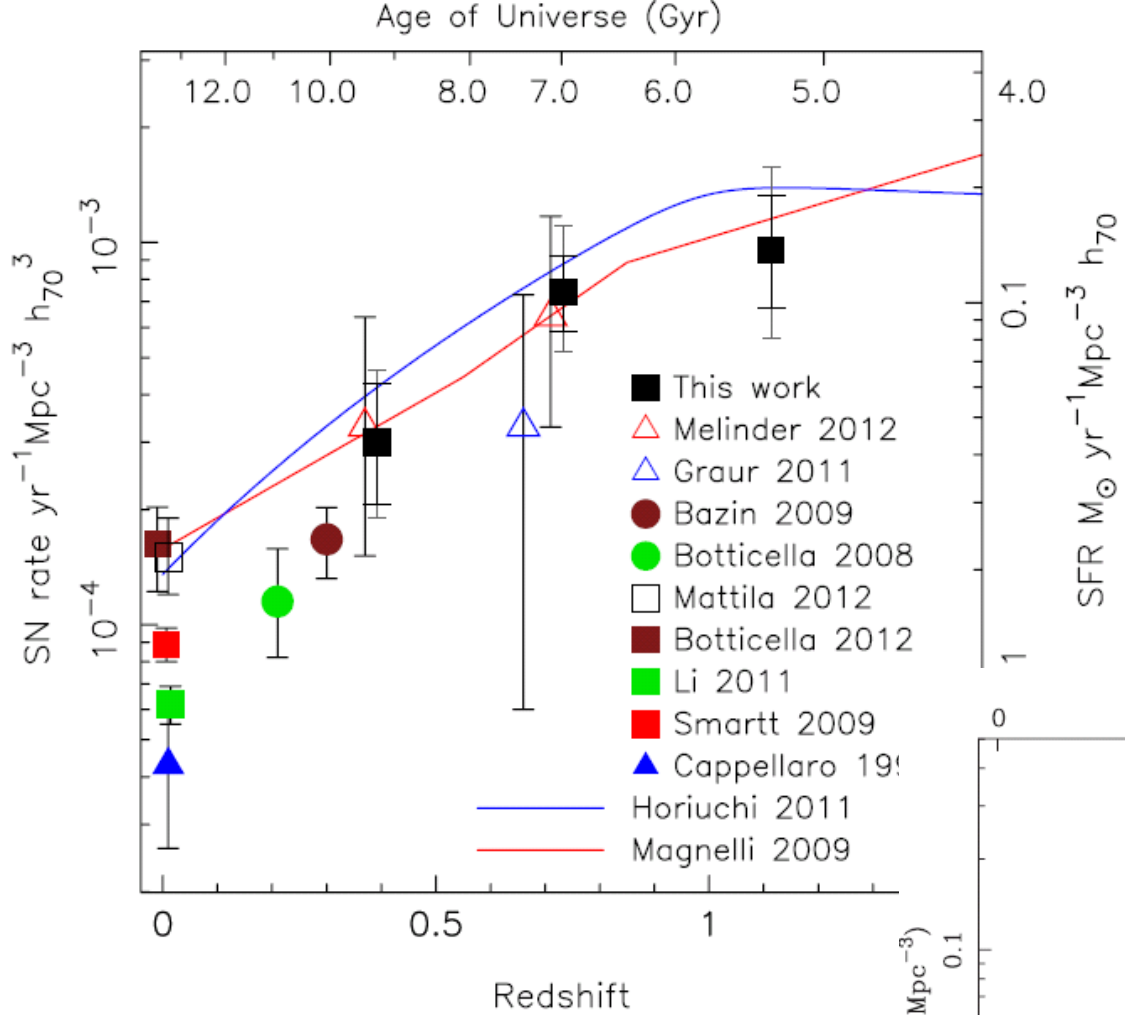


Dahlen et al. 2012

Hopkings & Beacom 2006

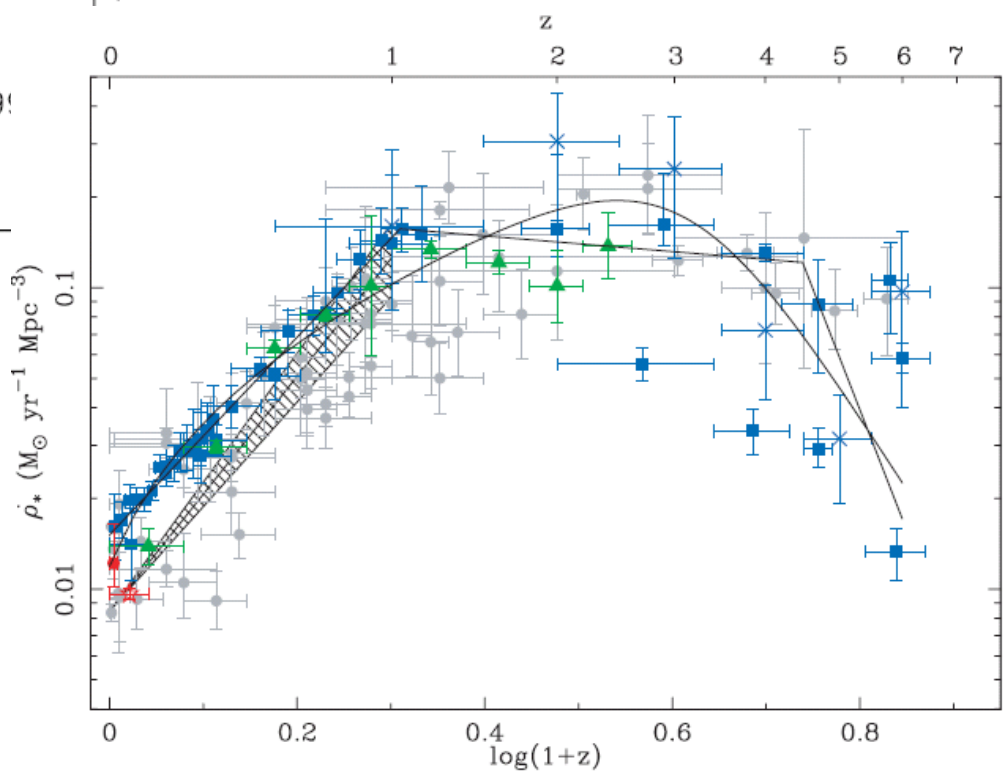

# Neutrino spectrum produced by IIn supernovae

$10^{-6}$ $(1+z)^{3.3}$ $Mpc^{-3}$ per year at z<1 - 1% of core collapse SNe

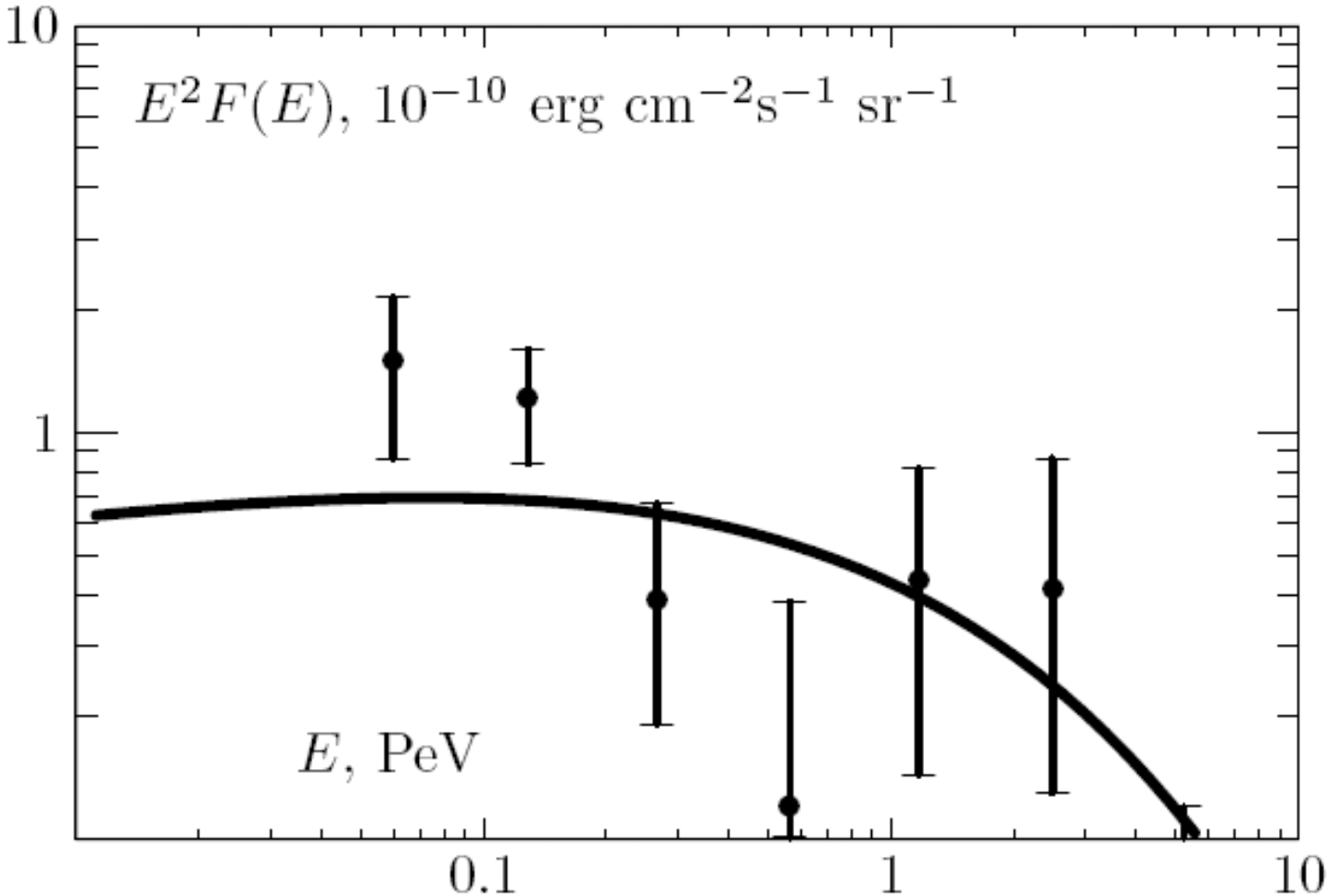

# Correlations of IIn SNe and IceCube neutrinos (~1 real correlation is expected)

1 correlation with 14 track events

SN 2005bx at 1.35 degree from the direction of track event 47

(chance probability 0.25)

1 correlation with 29 new track events (Aartsen et al. 2016)

SN 2005jq at 0.28 degree from the direction of track event 11

(chance probability 0.07)

# Estimate of neutrino flux from known IIn supernovae

Neutrino energy flux

$$E^2 F(E) = \frac{E^2 N(E)}{(4\pi)^2} \frac{1}{T} \sum_{SN} \frac{1}{D^2}$$

$$\sum_{SN} \frac{1}{D^2}$$ = 0.027 $Mpc^{-2}$ for T=10 years from SN cataloge

$E^2N(E) \sim 2\ 10^{49}$ erg in our modeling

$E^2F(E) = 10^{-12}$ erg $cm^{-2}$ $sr^{-1}$ - 2% of Icecube flux

# Summary

1. Non-resonant streaming instability produced by the electric current of run-away CR particles results in the significant magnetic amplification at fast SNR shocks.

2. Regular electric fields generated in the course of non-resonant instability suppress very efficient acceleration of particles producing the instability (protons). The acceleration of electrons is more efficient.

3. This effect is significant for shocks with velocities > 10000 km/s (and probably for relativistic shocks) propagating in the interstellar medium or for slower shocks propagating in the medium with weak magnetic fields.

4. Number of observed in gamma rays SNRs have enough CR energy power to explain the origin of galactic CRs. But modest maximum energies ~100 TeV for remnants of IIP SNe.

5. SNe IIn can be the sources of high energy neutrinos. The main contribution comes from z~1. Maximum energies of accelerated protons can reach $10^{17}$ eV. Remnants of these SNe can be Pevatrons.